[†]Now at Ibeo Automotive Systems, Hamburg, Germany

Key Points:

- Basal roughness at the onset of the NEGIS hints to a geomorphic anisotropy and a change in the geomorphological regime
- Basal water is funneled into the ice stream upstream and redistributed toward the shear margins further downstream
- A smooth and progressively lubricated bed reduces basal traction and favors the acceleration of the NEGIS at its onset

Correspondence to:
S. Franke,
steven.franke@awi.de

Complex Basal Conditions and Their Influence on Ice Flow at the Onset of the Northeast Greenland Ice Stream

Steven Franke[1] [iD], Daniela Jansen[1] [iD], Sebastian Beyer[1,2] [iD], Niklas Neckel[1] [iD], Tobias Binder[1,†] [iD], John Paden[3] [iD], and Olaf Eisen[1,4] [iD]

[1]Alfred Wegener Institute, Helmholtz Centre for Polar and Marine Research, Bremerhaven, Germany, [2]MARUM - Center for Marine Environmental Sciences, University of Bremen, Bremen, Germany, [3]Center for Remote Sensing of Ice Sheets (CReSIS), University of Kansas, Lawrence, KS, USA, [4]Department of Geosciences, University of Bremen, Bremen, Germany

Abstract The ice stream geometry and large ice surface velocities at the onset region of the Northeast Greenland Ice Stream (NEGIS) are not yet well reproduced by ice sheet models. The quantification of basal sliding and a parametrization of basal conditions remains a major gap. In this study, we assess the basal conditions of the onset region of the NEGIS in a systematic analysis of airborne ultra-wideband radar data. We evaluate basal roughness and basal return echoes in the context of the current ice stream geometry and ice surface velocity. We observe a change from a smooth to a rougher bed where the ice stream widens, and a distinct roughness anisotropy, indicating a preferred orientation of subglacial structures. In the upstream region, the excess ice mass flux through the shear margins is evacuated by ice flow acceleration and along-flow stretching of the ice. At the downstream part, the generally rougher bed topography correlates with a decrease in flow acceleration and lateral variations in ice surface velocity. Together with basal water routing pathways, this hints to two different zones in this part of the NEGIS: the upstream region collecting water, with a reduced basal traction, and downstream, where the ice stream is slowing down and is widening on a rougher bed, with a distribution of basal water toward the shear margins. Our findings support the hypothesis that the NEGIS is strongly interconnected to the subglacial water system in its onset region, but also to the subglacial substrate and morphology.

Plain Language Summary The Northeast Greenland Ice Stream (NEGIS) transports a large amount of ice mass from the interior of the Greenland Ice Sheet (GrIS) toward the ocean. The extent and geometry of the NEGIS are difficult to reproduce in current ice sheet models because many boundary conditions, such as the properties of the ice base, are not well known. In this study, we present new characteristics of the ice base from the onset region of the NEGIS derived by airborne radio-echo sounding data. Our data yield a smooth and increasingly lubricated bed in the upstream part of our survey area, which enables the ice to accelerate. Our results confirm the hypothesis that the position of the ice stream boundaries are coupled to the subglacial hydrology system.

1. Introduction

The lack of high-resolution bed topography and knowledge about the subglacial conditions in Greenland and Antarctica is one of the largest sources of uncertainty in present ice sheet projections (Morlighem et al., 2019) and higher resolution bed topography is needed to improve the accuracy of ice sheet models (Durand et al., 2011). The subglacial environment of the Antarctic and Greenland Ice Sheet (AIS, GrIS) is only poorly known from direct observations. The technical and logistical efforts for an analysis of the base underneath ice, often several kilometres thick, is much more challenging than observations on paleo-glaciated areas on land or the seafloor through remote sensing techniques (e.g., Clark and Meehan 2001; Stokes et al., 2013) or marine swath bathymetry (e.g., Arndt et al., 2020; Dowdeswell et al., 2004). Most of the knowledge about the ice covered bathymetry, bed topography and basal properties are deduced from the analysis and interpretation of indirect observations like radio-echo sounding (Fretwell et al., 2013; Humbert et al., 2018; Morlighem et al., 2019, 2017; Schroeder et al., 2019, 2020; Winter et al., 2017), seismic (Brisbourne et al., 2014; Dow et al., 2013; Hofstede et al., 2018; Kulessa et al., 2017; Rosier et al., 2018; Smith et al., 2020) as well as magnetic and gravimetric surveys combined with modeling approaches (An et al., 2019; Cochran & Bell, 2012; Eisermann et al., 2020; Muto et al., 2013). In the central regions of the

AIS and GrIS, little is known about the distribution and properties of bedrock, lithified and unlithified sediments, liquid water quantity, hydromechanical processes and the thermal and mechanical properties of ice (Clarke, 2005). Variations of these parameters over time can influence the spatial and temporal behavior of the ice sheets and their streams, by altering the fast flow dynamics or the mobilization of subglacial sediments. It is assumed that parts of the base of the GrIS are covered by mechanically weak sediments, which facilitate basal sliding (Christianson et al., 2014; C. F. Dow et al., 2013). Furthermore, an analysis of the thermal state of the base reveals large areas of a thawed bed and high melt rates at the interior of the GrIS (Fahnestock, 2001; Jordan et al., 2018; MacGregor et al., 2016). However, the response of changes at the glacier base to the ice surface dynamics can vary on several time scales (Ryser et al., 2014).

In Greenland, one feature causing the most significant discrepancies between numerically modeled and observed ice surface velocities is the Northeast Greenland Ice Stream (NEGIS) (Aschwanden et al., 2016), which therefore represents one of the largest uncertainties for ice flow predictions. Several studies assessed the genesis as well as the positioning and geometry of the NEGIS in its onset region close to the ice divide (Fahnestock, 2001; Fahnestock et al., 1993; Joughin et al., 2001). The ice stream is constrained by its 400-km-long shear margins, and their locations at its onset region show no apparent indications for a topographic control (Franke et al., 2020b; Holschuh et al., 2019). Christianson et al. (2014) established an extended hypothesis on the initiation and development of the NEGIS based on these studies and an analysis of data from an extensive geophysical survey at the onset of the ice stream, centered at the drill site of the EGRIP ice core where the ice stream widens (Vallelonga et al., 2014). The ice stream is most likely initiated by anomalous high geothermal heat flux (GHF) close to the ice divide (Fahnestock, 2001). The GHF is the primary control on the generation of basal meltwater and the sensitivity of the hydrology system (Smith-Johnsen et al., 2020). In the absence of cross-marginal ice flow, acceleration along the trunk of NEGIS should lead to the development of a surface trough. However, the lack of an observed trough must mean acceleration is compensated by an influx of ice through the shear margins (Christianson et al., 2014). The increasing ice flow velocity of the onset of the NEGIS in its current geometry would lead to the development a surface trough, which is not consistent with observations.

In present ice-sheet models, the NEGIS is reproduced through estimating basal-shear stress from inverse methods informed by surface velocities (Larour et al., 2014; Smith-Johnsen et al., 2019). Estimates of basal resistance are not accurate enough to sufficiently reproduce geometry and surface velocities of ice streams by ice-flow models, as our understanding of processes and conditions is still very limited. In this regard, the analysis of the basal roughness has become important for glacial geomorphological research and is an increasingly accepted attribute to describe subglacial conditions and to derive a controlling factor for the dynamics of ice-sheets (Smith et al., 2013). Basal roughness parameters can thus help us to discriminate whether the ice is underlain by softer sediments or harder rock, to reveal traces of former ice dynamics, to constrain the thermal regime and identify potential processes of subglacial erosion and deposition of sediments (Bingham & Siegert, 2009). They are key parameters for the ice—bed coupling (Hughes et al., 2011), to model basal sliding (Wilkens et al., 2015) as well as a parameter for subglacial hydrology studies (Meyer et al., 2018). At present, the roughness of the bed topography is typically analyzed by spectral analysis of vertical and horizontal topography variations, based on the approaches of Shepard et al. (2001), Taylor et al. (2004), and Li et al. (2010). In many studies, basal roughness shows a clear correlation to basal drag and ice sheet velocity (Smith et al., 2013). In radio-echo sounding measurements, the roughness of the subglacial topography on different scales also influences the scattering of reflected radar waves (Jordan et al., 2017) and, thus, the reflectivity of the bed (Jacobel et al., 2010). Furthermore, the intensity and reflection pattern of the bed return informs us about the reflection properties of the base, thus complementing inferences made by the roughness parameter. Jordan et al. (2017), for example, analyze the radar scattering in combination with the topographically derived roughness to evaluate the relationship between basal roughness and the basal thermal state. The study concludes that frozen regions are relatively smooth and many thawed regions are relatively rough.

The majority of subglacial roughness studies in Antarctica focus on outlet glaciers (Bingham & Siegert, 2007, 2009; Diez et al., 2018; MacGregor et al., 2013; Rippin et al., 2011, 2014, 2006; Taylor et al., 2004) with only a few studies extending over large areas (e.g., Eisen et al. [2020] in East Antarctica). In a study to model the surface flow field of Pine Island Glacier, Wilkens et al. (2015) related basal sliding to a bed roughness

parameter and were able to reproduce some essential flow features, like the location of the fast-flowing central stream and various tributaries. One of the first studies of basal roughness in Greenland was conducted by Layberry and Bamber (2001) using the residual bed elevation deviation to quantify basal roughness. An estimate of the basal roughness distribution based on a spectral approach for those part of GrIS covered by radio-echo sounding data was given by Rippin (2013). A recent study by Cooper et al. (2019) indicates different relationships between ice flow and basal roughness parameters. They conclude that in certain regions of slow ice flow, coinciding with low vertical roughness (i.e. smooth topography), a mechanism other than basal sliding must control ice flow. The relation between basal traction and sliding is still under debate and varies for different glaciological settings. For example, the study of L. A. Stearns and van der Veen (2018), observed that bed friction, which should control basal sliding, does not control the rapid flow of a large number of glaciers in Greenland. For a full account of the discussion also see the subsequent replies to the study (Minchew et al., 2019; Stearns & van der Veen, 2019). Furthermore, the inverse correlation between basal roughness and ice-sheet flow velocity (slow-flowing areas are mostly smooth, while increased ice flow shows rougher beds) encouraged the authors of more recent studies to rethink the influence of basal roughness to basal traction (Rippin, 2013). Possible mechanisms that control basal traction could be the thermal state at the base, subglacial hydrology and the rates of erosion and deformation of sediments.

In this paper, we use airborne radar data from AWI's ultra-wideband radar system to analyze the basal conditions of the onset of the NEGIS. We perform a spectral roughness analysis to characterize the pattern of the bed return signals and investigate the subglacial roughness parallel and perpendicular to ice flow. For the basal roughness analysis on finer spatial scales, we analyze the scattering pattern of the bed return echoes. Based on an improved bed elevation model, we investigate subglacial water pathways. We then combine these data with an analysis of ice mass flux at the ice stream. This should ultimately give a consistent picture of the processes at the base, which control ice flow dynamics. Finally, we use our larger-scale data set to discuss the extended hypothesis of Christianson et al. (2014) of the initiation and development of the NEGIS as well as the positioning of the shear margins in its onset region.

Our results reveal a regional change in basal roughness and the pattern and intensity of the basal return echo from the upstream toward the downstream part in our study area on the NEGIS (Figure 2). Furthermore, we detect a bed roughness anisotropy concerning the ice flow direction, indicating streamlining parallel to ice flow. The analysis of water flow paths on the basis of a better resolved bed topography confirms the hypothesis that the subglacial hydrology and the position of the shear margins are tightly coupled.

2. Data and Methods

2.1. Survey Area and Data Acquisition

We use airborne radar data of the EGRIP-NOR-2018 survey in the onset area of the NEGIS (Figure 1). The data were collected with the AWI multi-channel ultra-wideband (UWB) airborne radar sounder (for details see Arnold et al., 2019; Franke et al., 2020b; Hale et al., 2016) and recorded at a center frequency of 195 MHz and a bandwidth of 30 MHz. The transmit signals are chirp waveforms transmitted at three stages with different pulse durations and gains to obtain high signal-to-noize ratio (SNR) in all parts of the radargrams. Radar data processing comprises pulse compression, along-track SAR processing (fk-migration) and cross-track array processing. A complete methodological description of the radar data processing and uncertainty estimation is described in Franke et al. (2020b). In the study area, the NEGIS accelerates from ~10–80 m/a over a distance of roughly 300 km and widens from ~20 km in the upstream boundary of our survey area to ~65 km further downstream (Figure 1). More than 8,000 km of survey profiles are distributed over an area of more than 250 km along ice flow direction and 50–100 km across, covering the interior of the ice stream, the shear margins and the slow-flowing area in the vicinity of the NEGIS (Figure 1). The profile spacing of across-flow profiles is 5 km in the central part of the survey area, near the drill site of the East Greenland Ice-core Project (EGRIP; http://eastgrip.org), and 10 km further upstream and downstream. Along-flow profiles are mostly aligned along calculated pathways of ice flow based on the velocity field of Joughin et al. (2017). For the rest of this paper, we will refer to upstream and downstream as the regions upstream and downstream of the EGRIP drill site, respectively.
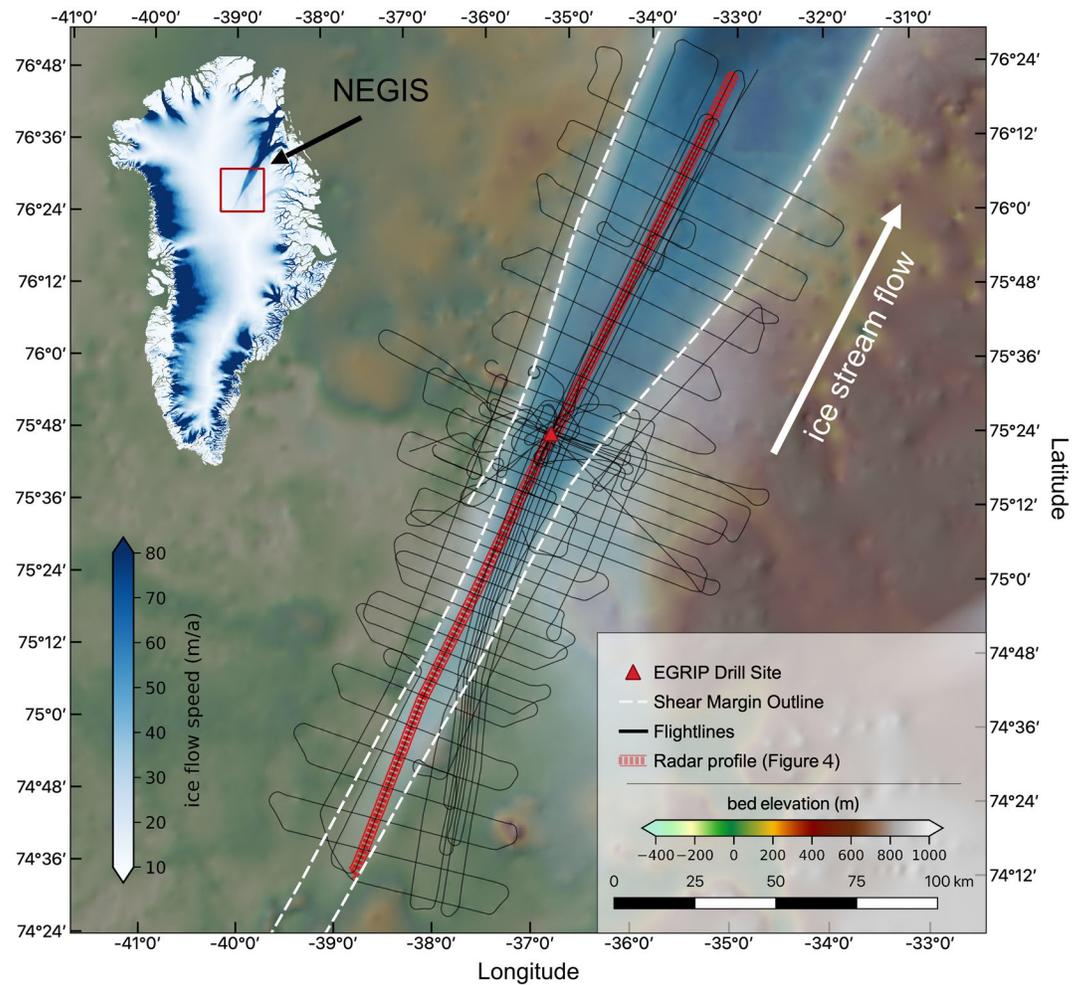
Figure 1. Overview of the survey area in the interior of the Greenland Ice Sheet at the onset of fast flow of the NEGIS. The black lines, which are centered at the EGRIP drill site, represent the survey profiles of the EGRIP-NOR-2018 airborne UWB radar survey (Franke et al., 2020b). The white dashed lines show the outline of the shear margins (determined from satellite imagery) and the dashed red line the radar profile shown in Figure 4. Bed elevation is referenced to mean sea level (EIGEN-6C4 geoid (Förste et al., 2007), this reference applies to all other maps showing the bed elevation) and ice flow velocity is based on the data set of Joughin et al. (2017) and is shown in blue color code for velocities larger than 10 m/a. The projection of this map and all following maps are shown in the coordinate system EPSG 3413 (WGS84/NSIDC Sea Ice Polar Stereographic North).

2.2. Basal Roughness Calculation

We define basal roughness as the relative vertical and horizontal variation of the topography of the ice-bed interface. In our analysis we calculate two parameters (ξ and η), which are commonly used to characterize basal roughness (Cooper et al., 2019; Gudlaugsson et al., 2013; Li et al., 2010; Rippin et al., 2014):

1. ξ reflects the vertical irregularity of the bed and provides information about the dominating vertical amplitudes. This roughness parameter is defined as the integral of the wavenumber spectrum over the range of a moving window (MW). Values close to 0 reflect the dominance of smaller amplitudes and a smoother topography.

2. Li et al. (2010) introduced the frequency roughness parameter η, which is calculated by dividing the vertical roughness ξ by the roughness of the bed slope ξ_{sl}. This parameter reflects the horizontal variation pointing out the dominance of a particular wavelength. High values represent the dominance of longer wavelength and smaller values the dominance of shorter wavelength.
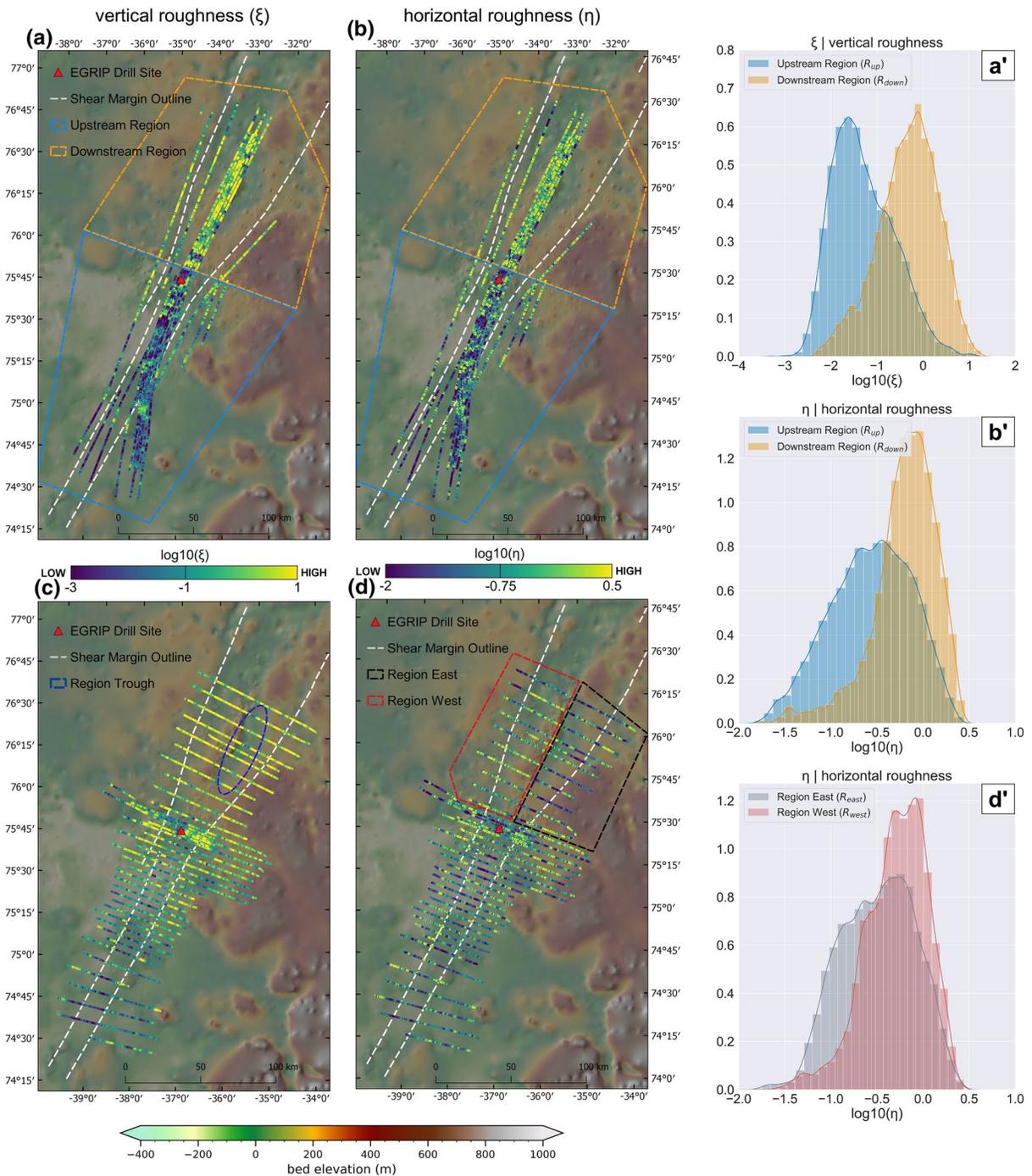
Figure 2. Survey area at the NEGIS showing (a) along- and (c) across-flow profiles of the vertical roughness parameter ξ and the horizontal roughness parameter η in (b) along and (d) across-flow profiles respectively. Both parameters are shown on a logarithmic scale. The background map represents the EGRIP-NOR-2018 bed topography of Franke et al. (2020b) in meters, referenced to mean sea-level (EIGEN-6C4 geoid). Histograms a' and b' show the distribution of ξ and η for the along-flow profiles for the upstream and downstream region, respectively (orange and blue outline in a and b). The y-axis on the histograms represents the kernel density estimation. The distribution of η in the western and eastern part of the downstream region (red and black outline in d) are shown in a histogram d'.

We use the bed picks of the EGRIP-NOR-18 data set (Franke et al., 2019, 2020b) for basal roughness calculation. The roughness analysis in this paper is based on the approaches of Hubbard et al. (2000) and Taylor et al. (2004) and uses a Fast Fourier Transform (FFT) to analyze the wavenumber spectra of variations in topography (Gudlaugsson et al., 2013). This requires a uniform sampling interval of data points on the bed elevation profiles. Synthetic Aperture Radar processing of our radar data already includes the creation of a new coordinate system with a constant spatial sampling interval for the focused radar data. The average spacing between data points is 14.78 m. For each data point on a linearly detrended profile, we calculate the wavenumber spectrum over a MW of 2^N data points. We test two different MW for our analysis: (i) $\sim$400 m, which corresponds to 32 data points ($N = 5$) and (ii) $\sim$2,000 m, which corresponds to 128 data points ($N = 7$). For the 32-data point MW, one data point covers the roughness at a resolution which is finer than the cell size of 500 m used for the bed elevation data sets of Morlighem et al. (2017) for Greenland and the NEGIS onset region by Franke et al. (2020b). To make sure that this small MW does not suppress long-wave structures, we compared the result of the 500 m MW with the results obtained for the $\sim$2,000 m MW. The comparison shows that significant changes are represented in both MWs. Because we focus on regions where clusters of high or low roughness values or trends appear, we use the larger ($N = 7$) MW for further analysis. For this manuscript, we will refer to this kind of basal roughness as *large-scale* roughness.

Because the interpretation of roughness parameters is highly directionally dependent and the dominating factor influencing bed formations is the direction of ice flow as shown by Falcini et al. (2018), Gudlaugsson et al. (2013), and Rippin et al. (2014), we separately analyze along- and across-flow profiles. We present roughness values on a logarithmic scale to emphasize the range of up to four orders of magnitude.

2.3. Ice Mass Flux

In order to calculate the ice mass flux in the survey area we employed 20 flux gates orientated perpendicular to the ice flow direction. These are limited by 19 additional flux gates along each shear margin forming 19 closed boxes. Following Neckel et al. (2012) the ice flux through each gate is calculated by

$$F = \sum_{i=2}^{i=N-1} v_i(\phi_i') H_i d_i \tag{1}$$

with N being the number of pixels in the flux gate and ϕ'_i the normal angle to the flux gate at position i. The ice flow velocity, ice thickness and pixel spacing are indicated by v_i, H_i, and d_i, respectively. In order to translate volume flux into mass flux, we employed an ice density of 910 kg m^{-3}.

We consider the full ice column for the analysis of the flux gate balance and calculate the ice fluxes as if there is no basal drag (plug flow). As input data, we use the ice surface velocity data from Joughin et al. (2017) and the ice thickness data from Franke et al. (2020b). Because we make only a large-scale interpretation of the mass flux in our survey region, we neglect surface and basal mass balance.

2.4. Basal Return Power

We use the intensity of the return echoes from the basal interface as an additional parameter to analyze the basal conditions at the onset region of the NEGS. We follow the approach of Jordan et al. (2016) and Jordan et al. (2017), which is based on the method developed by Oswald and Gogineni (2008) and Oswald and Gogineni (2012). The return power is calculated from an along-track average of the basal return echo and is defined as the integral over a window of samples that represent the reflected energy from the bed (Equation 2). Before arithmetically averaging along-track, we use the bed picks of Franke et al. (2020b) to shift the bed reflection to a single level. The arithmetical averages are phase-incoherent, but help to reduce fading effects and to smooth power fluctuations (Oswald & Gogineni, 2008). We tested different values for along-track averaging and chose a value of 50 (two times 25 adjacent traces). With this value the power fluctuations are small enough to analyze as many tracks as possible, but also not too low, so that the signal is not smoothed too much. The size of the range window is kept variable and is set for a threshold above 3.5% the noise floor for a section above the bed reflection. The upper boundary is defined where the signal starts to be above the threshold and the lower boundary where the signal drops for the first time below this

threshold (for further details, see Figure 3 in Jordan et al., 2016). We follow Jordan et al. (2016) and define the integrated power P_{int}, referred to as the bed return power (BRP), by

$$P_{int} = \int_{L_{upper}}^{L_{lower}} P(L_i), \qquad (2)$$

with the upper and lower limit of the integration window threshold L_{upper} and L_{lower}, the return power of a sample P and the depth range index L_i. The full waveform of the basal return in the integration window represents an overlay of the specularly reflected energy from nadir and scattered energy from along- and cross-track off-nadir (Young et al., 2016). The majority of the scatter from off-nadir will arise from across-track reflections because SAR post-processing reduces the footprint of return signals in along-track (Raney, 1998). Similar to the approaches of Jordan et al. (2016) and Jordan et al. (2018), we implement additional quality control rules. Traces where the window for the integration of depth-range bins was smaller than five range bins were abnormally thin and abrupt reflections associated with clutter and were removed. The maximum size of the integration window is set to 40 range bins to limit the amount of far off-nadir layover signals.

The radar wave bed return power is corrected for spherical spreading and therefore depends mainly on the properties of the ice-bed interface, scattering properties of the bed, anisotropy in the ice fabric and dielectric attenuation within the ice column. The largest energy loss is related to dielectric attenuation, which depends on ice temperature, chemistry and other impurities in the ice column (Corr et al., 1993; Matsuoka, 2011). If dielectric attenuation varies significantly, the distinction between basal water and dry sediment is difficult because the effect of englacial attenuation can be much more significant than the contrast in reflectivity between a wet and dry base (Matsuoka, 2011).

No ice sheet models exist so far to accurately reproduce ice flow and englacial temperature in the rather complicated region of the NEGIS ice stream with its distinct shear margins. Therefore, we apply a simple linear fit between bed power and ice thickness to obtain the average attenuation rate. Based on this fit, we correct for englacial attenuation with a constant value of 8 dB per km ice thickness. However, this correction will only remove the depth-correlated component of the bed reflection power.

The correction factor depends mainly on ice temperature, which in turn depends on the geothermal heat flux (GHF), the mean annual air temperature, surface accumulation rates and frictional heating at the glacier bed and from internal ice deformation. Estimates on GHF vary significantly and are associated with large uncertainties (Rogozhina et al., 2012). Other radar studies investigating BRP at the NEGIS find different values to correct for englacial attenuation. Christianson et al. (2014) found attenuation rates from a linear fit between bed power and ice thickness at the onset of the NEGIS of 8 dB/km. Attenuation rates at the NEGIS onset in the Greenland wide study of (Macgregor et al., 2015) are larger than 12 dB/km, but show an increasing uncertainty toward the ice sheet margin. The overall resulting depth-averaged attenuation rate of the common midpoint survey of Holschuh et al. (2016) are up to 3 times higher (27 db/km) than the attenuation rates found in the previous studies.

2.5. Waveform Abruptness

The intensity of the integrated bed return echo as well as the length of the integration window is sensitive to small-scale variations in basal roughness (Cooper et al., 2019), which are not resolved in the radar measurements and depend on the size of the Fresnel zone. The diameter of the Fresnel Zone for a bandwidth of 180–210 MHz and an ice thickness range of 2–3 km is ~ 60 m. Ice-bed interface roughness and the wavelength of the radar signal determines the nature of the electromagnetic scattering. However, rough subglacial terrain can produce side reflections, which are difficult to separate from the nadir bed echo return. In this case, the footprint of the radar signal and consequently the area of the basal backscatter is larger than the Fresnel zone and determined by the beam angle of the transmitted signal. To characterize the basal scattering, we follow the approach of Oswald and Gogineni (2008) which has been adapted and extensively used in Greenland by Cooper et al. (2019), Jordan et al. (2016, 2017), and Jordan et al. (2018) analyzing the waveform abruptness of the bed reflection. We follow Cooper et al. (2019) and define the abruptness parameter A by
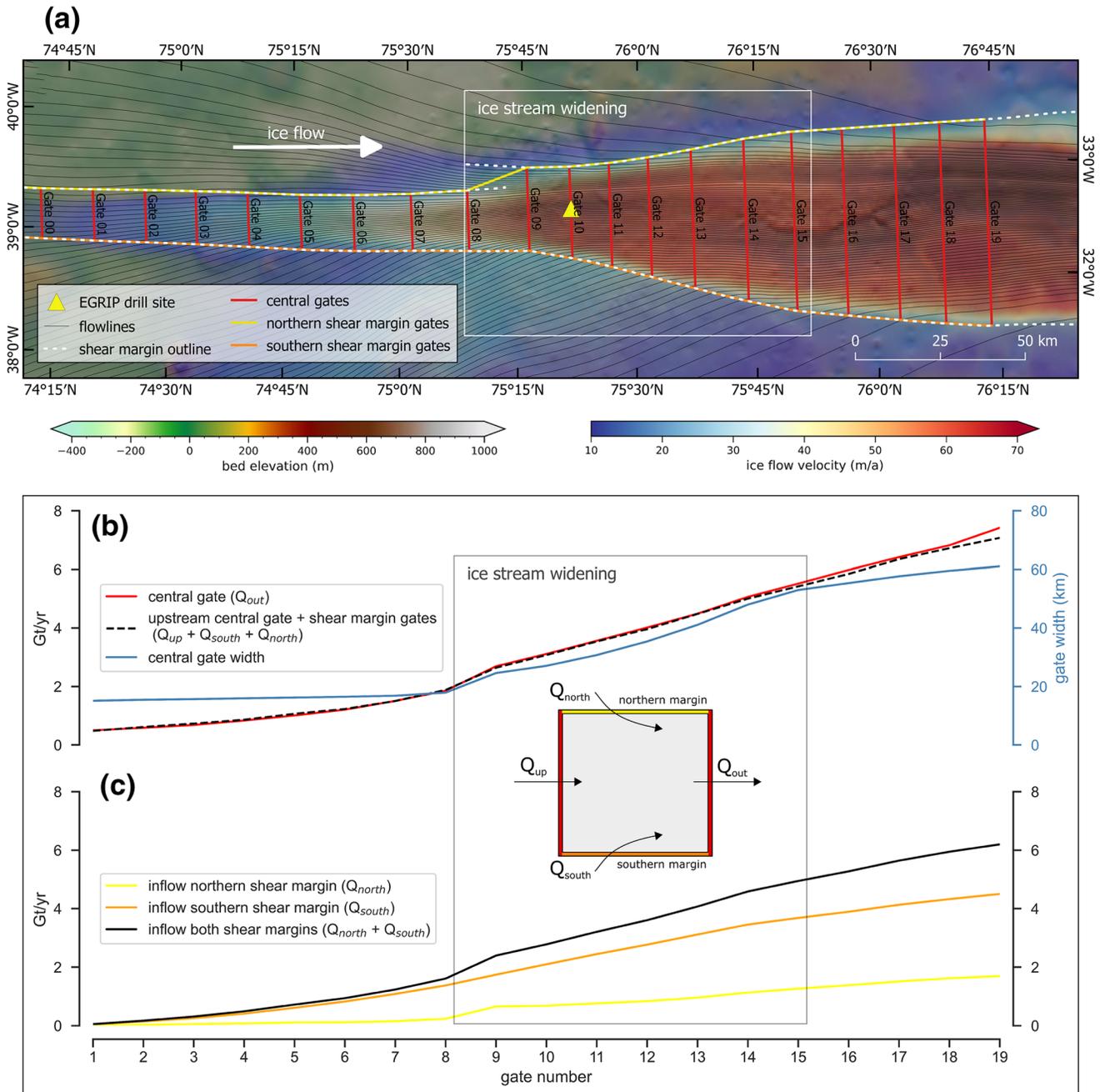
Figure 3. Flux gate analysis of the onset of the NEGIS. Panel (a) shows the position of central flux gates (red) and flux gates at the shear margins (yellow and orange, respectively). The location where the ice stream widens is marked with a white outline. Panel (b) shows the mass flux (in Gt/yr) through the central gates (Q_{out}; red line) in comparison to the sum of the respective upstream central gate (Q_{up}) and the corresponding shear margin gates ($Q_{south} + Q_{north}$; black dashed line). The blue line represents the width of the central gates. The cumulative mass flux through the northern and southern shear margin (as well as the sum of both) is shown in panel (c).

$$A = \frac{P_{\max}}{P_{\text{agg}}}, \tag{3}$$

where $P_{\max}$ is the maximum amplitude of the basal return echo in the integration window and P_{agg} the integrated basal return power (Oswald and Gogineni, 2008). A large $P_{\max}$ in a small integration window will result in a large value of A. If the reflected energy is distributed over a larger integration window, it

will decrease the maximum amplitude and result in a small value of A (for details see Figure 4 in Cooper et al., 2019). High values indicate an abrupt return (i.e., along-track focusing was sufficient to recover energy to the nadir reflection point), whereas low values indicate a broad return (likely due to energy recovered from a range of cross-track angles, which could not be focused due to the narrow antenna array in the cross-track direction). We will refer to this scattering-derived roughness as *small-scale* roughness because it represents roughness of a different scale and type than the spectral *large-scale* roughness.

2.6. Basal Water Routing

We compute (potential) subglacial water pathways from the hydrological potential F. We assume that the water flow depends on the elevation potential and the water pressure r_w (Shreve, 1972). Under the assumption of equilibrium between water pressure and ice overburden pressure we can write

$$\Phi = \rho_w g b + \rho_i g H, \qquad (4)$$

where ρ_w is the density of water, g is the acceleration due to gravity, b is the bed elevation, and H the ice thickness (Le Brocq et al., 2009; Livingstone et al., 2013). We apply a simple flux routing scheme as described by Le Brocq et al. (2006) to successively compute the number of upstream cells (cells that potentially contribute water to this cell) for each grid cell. The equilibrium assumption in Equation 4 is only valid at large scales (km) and makes the potential especially sensitive to the ice surface gradient. Hence, this method cannot account for localized water flow, such as flow through channels (more details on our implementation can be found in Calov et al., 2018). We make use of bed topography and ice thickness data of the EGRIP-NOR-2018 bed elevation model from Franke et al. (2020b) as well as the BedMachine v3 topography (Morlighem et al., 2017; BMv3). We use both models as input fields to analyze the sensitivity of subglacial water routing to the bed topography. While this method allows for using basal melt rates as input to quantify transported water volumes, we chose to simply count the number of upstream cells as a measure for potential water pathways. Basal melt rates are poorly constrained for this area, in particular, because the spatial variations in geothermal heat flux are subject to considerable uncertainties (Dow et al., 2018; Jordan et al., 2018; Smith-Johnsen et al., 2019). Nevertheless, we can use the water pathways to estimate the distribution of basal water, particularly for areas where we can infer a thawed base and the generation of meltwater by other methods. Several studies have detected or modeled water at the base of the Greenland Ice Sheet, but the amount of basal water is uncertain and difficult to measure (Fahnestock, 2001; Jordan et al., 2018; MacGregor et al., 2016).

3. Results

3.1. Spatial Distribution of Spectral Basal Roughness

We analyzed $\sim$ 370,000 data points for vertical and horizontal roughness with a spectral analysis approach and present our result as the dominating vertical amplitude (ξ) and horizontal wavelength (η) over a 2,000 m MW in along-flow and across-flow profiles in Figure 2. We observe that high ξ, in general, correlate with higher η values. Also, the correlation of ξ and η shows higher vertical roughness values for the same horizontal roughness in cross-flow profiles compared to along-flow profiles. On the linear scale, vertical roughness values vary on the order of four magnitudes and horizontal roughness in the order of 2.5. Basal roughness values show distinctly different spatial patterns, independent of flight-line orientation, in two areas: upstream and downstream of the EGRIP drill site (Figure 2). We will refer to these two regions as R_{up} (upstream) and R_{down} (downstream), respectively, and will present their particular characteristics in the following.

Region R_{up} shows low vertical and horizontal roughness values for profiles along- and across-flow. On average, ξ and η are small for profiles along-flow in the ice stream, while we observe an increase of ξ for profiles perpendicular to flow when moving from the upstream end in the south-west toward the EGRIP drill site. Across-flow profiles show distinctly different roughness values within and outside of the ice stream. Outside of the south-eastern shear margin, η is higher than inside the ice stream. Along-flow profiles that

are located outside of the ice stream show similar horizontal and vertical roughness values as along-flow profiles in the ice stream. The statistical distribution of roughness values for both, ξ and η, for across-flow profiles is much wider. However, it has to be noted that the profiles also extend further to the South-East and North-West here than further upstream.

The bed elevation in the transition area rises about 500 m in flow direction and the average ice thickness decreases 400 m compared to the region R_{up}. The transition zone between regions R_{up} and R_{down} is characterized by a dominance of lower vertical amplitudes (ξ) and shorter horizontal wavelengths (η). Both the vertical and horizontal roughness values are, on average, higher for along and across flow profiles in the downstream region R_{down} in comparison to the upstream region R_{up}. Along-flow profiles show a strong increase in ξ and η, and both remain high in value with little variability. Along profiles perpendicular to ice flow, ξ shows a trend toward increasing values downstream and at the upstream end of region R_{down}. The horizontal roughness η shows two different domains for across-flow profiles. Low values of horizontal roughness dominate in the south-eastern part of region R_{down}, which we will refer to as region R_{east}, and high values in the north-western region R_{west} (Figure 2d). The transition from high to low values between these two sub-regions, which we will refer to as R_{trough} (Figure 2c), coincides with the steep eastern flank of a central ridge as well as with a local topographic low (Franke et al., 2020b). In the region R_{trough} we observe low vertical roughness values in the center and higher roughness values at the edges of the region. For region R_{down}, along-flow profiles located outside of the ice stream, show a similar development in both, ξ and η (Figures 2a and 2b). For the parts of across-flow profiles, which are located outside of the shear margin, we detect the same trend of increasing vertical roughness from upstream to downstream (Figure 2c), but not in the horizontal roughness which is highly variable on across-flow profiles outside the shear margins.

3.2. Development of Ice Stream Flux in a Kinematic-Geometrical Context

For an interpretation of subglacial properties and ice stream development, we consider a flux balance, a development of englacial units along ice flow and the change of width and lateral surface velocity along the ice stream.

The flux gate analysis focuses on (i) the comparison of the mass flux though a central gate (Q_{out}) to the sum of mass flux of the upstream gate and the respective shear margin gates ($Q_{up} + Q_{south} + Q_{north}$; shown schematically in Figure 3 b/c) as well as (ii) the cumulative mass flux through the shear margins, which shows the following features:

1. Upstream of the EGRIP drill site (gates 1–8) the ice stream has a constant width and ice mass flux increases and we observe an acceleration of the ice surface speed. The initial mass flux at gate one is relatively small and Figure 3c indicates that most of the additional mass flux is provided through the southern shear margin.
2. Between gates 8 and 15, the ice stream widens. Total mass flux increases constantly, with a small step due to the shift northward of the northern shear margin. The widths of the central gates increase, and thus, provides the ice stream with additional mass flux through the shear margins.
3. After gate 15, the widening rate of the ice stream decreases but the flux gates indicate no change in mass flux.

We use two isochrones in a central radar profile as boundaries to define two englacial units. Figure 4a shows this radar profile, which is oriented along-flow at the location indicated in Figures 1 and 5 with a red line. This radar section is composed of two profiles and was concatenated at the location of the EGRIP drill site. The profile from 0 to 160 km will be referred to as the upstream section and the profile from 160 to 280 km as the downstream section. There is an offset between the two profiles of 1 km across-flow. For both sections, we tracked two internal reflection horizons, which have a respective age of ∼30 and 52 ka, respectively, which we transferred from dating of radar reflections at the location of the NGRIP ice core (Vallelonga et al., 2014). We will refer to the thickness of these two layers as the basal unit between the 52 ka horizon and the bed reflection; and the internal unit between the 30 ka horizon and the 52 ka horizon, respectively. The upstream section shows an increase of ice surface velocity (Figure 4b) from 12 to 58 m/a over a distance of 150 km. Vertical and horizontal roughness (Figures 4c and 4d) are on average low but vary over two to three orders of magnitude. Furthermore, the thickness of the internal and basal unit remains nearly con-
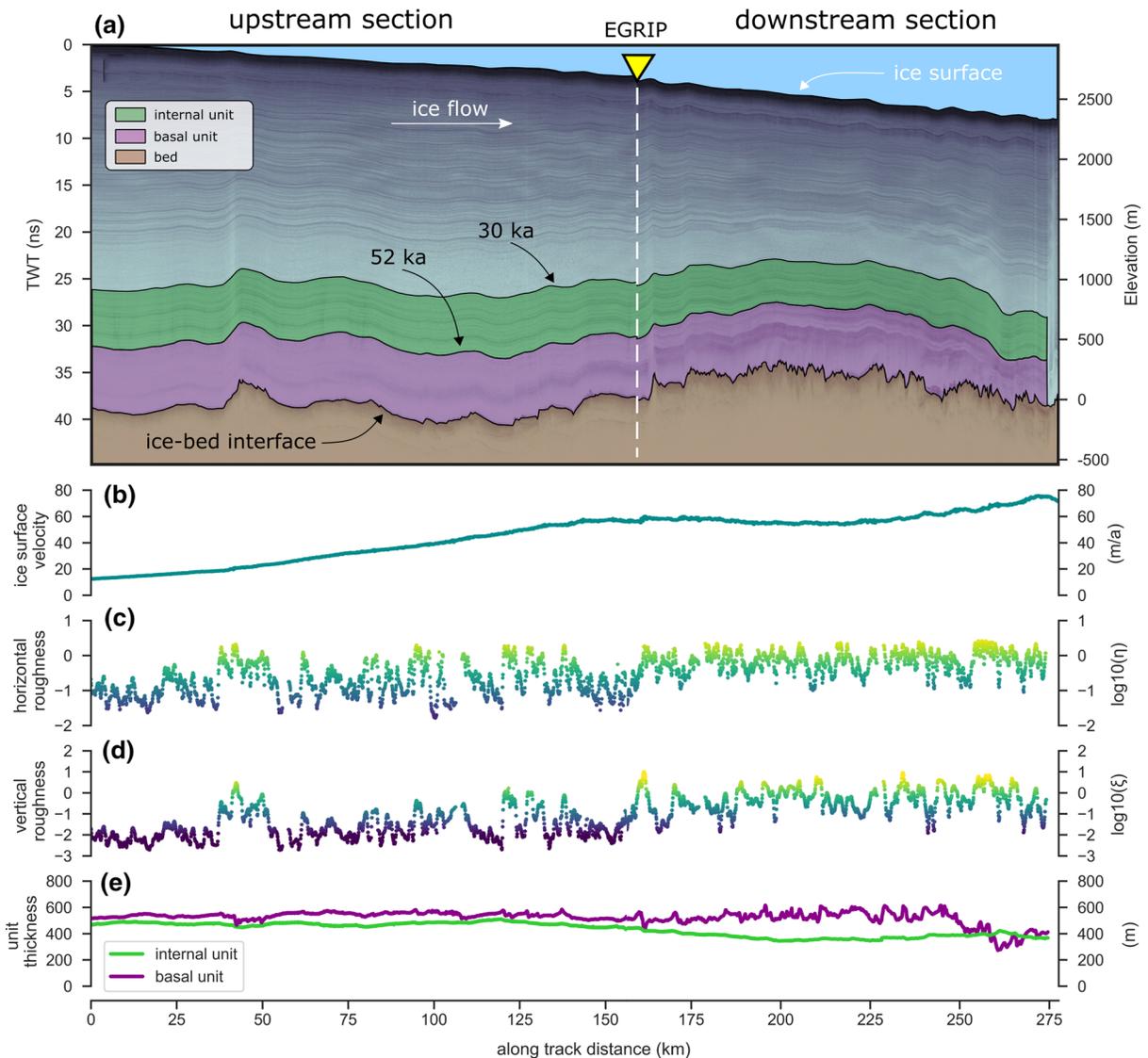
Figure 4. Evolution of several basal and englacial properties in ice flow direction, extending from far upstream to the downstream end of our survey area (red line in Figures 1 and 5). Because there is no continuous survey profile, the downstream part (right part of the dashed line) is offset ∼1 km to the South-East (transverse to along-flow profile orientation) relative to the upstream profile (left of the dashed line). The transition between the two profiles marks the position of the EGRIP drill site (yellow triangle). Ice flow direction is from left to right. (a) along-flow radargrams with continuously tracked surface, two internal ice units (basal unit in purple and internal unit in green) and bed reflection; (b) ice surface flow velocity; (c) horizontal roughness η and (d) vertical roughness ξ, both with the same color code and scaling as in Figure 2; and (e) the thickness of the internal and basal unit.

stant in the upstream section (Figure 4e). In the downstream section, between 150 and 175 km, we observe a decrease of the internal unit thickness of ∼125 m, whereas the basal unit thickness remains constant downstream to 240 km. The surface velocity in the downstream section shows a small decrease between 175 and 210 km and increases thereafter to ∼80 m/a. Vertical and horizontal roughness in the downstream section is higher on average than in the upstream section. The increase in roughness correlates with a decrease in ice surface velocity and also with a decrease in the thickness of the ice column. The internal unit becomes thinner while the thickness of the basal unit remains constant.

Figure 5 shows the downstream section and the spatial distribution of ice surface velocity, flow lines indicating the flow path (Figure 5a) of a point on the ice surface, as well as vertical and horizontal roughness (Figures 5b and 5c respectively). Surface flow velocity is about 5–8 m/a higher in the eastern part of the section than in the western part. The area of increased ice surface velocity correlates with the location of
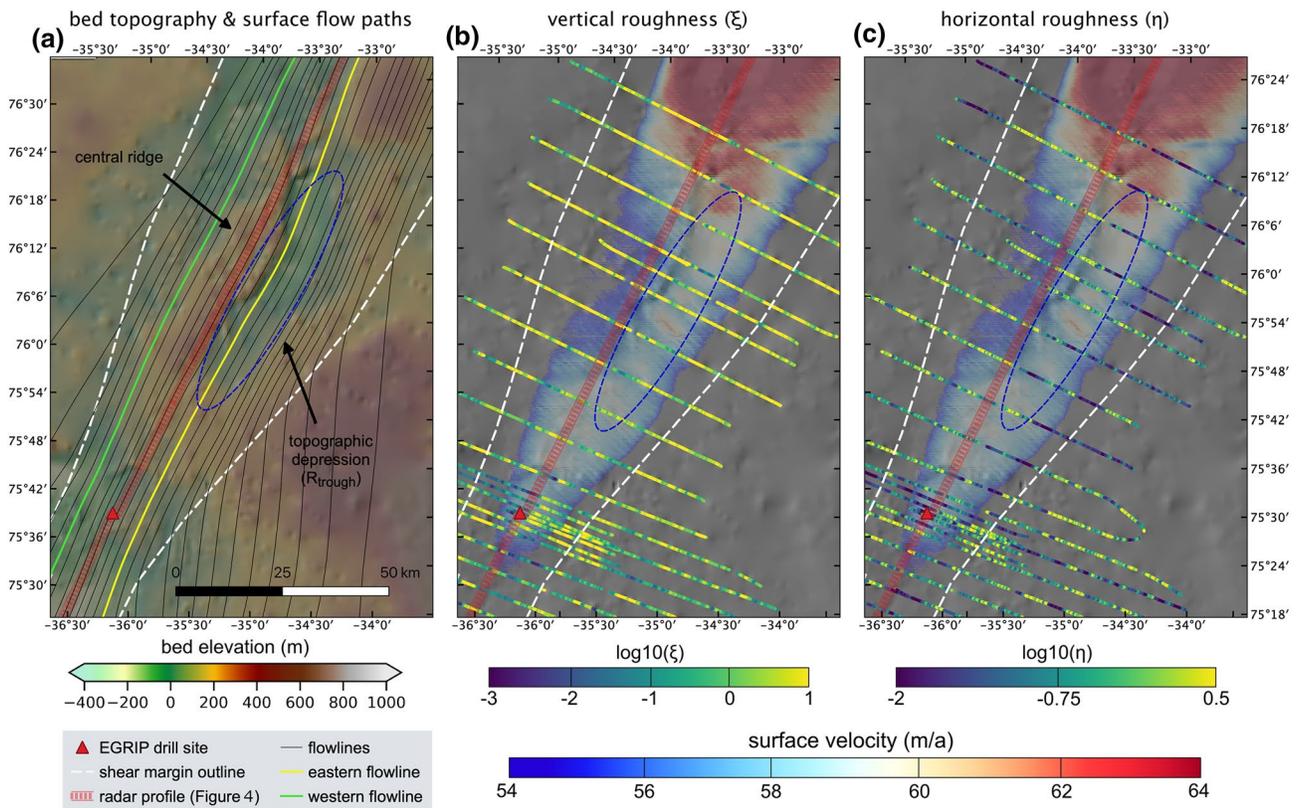
Figure 5. Bed and flow properties in the downstream survey region, North-East of the EGRIP drill site (red triangle). Panel a shows the bed topography and flowlines of the ice surface (ice flow direction is toward North-East as indicated in Figure 1). Panel b shows the vertical roughness parameter ξ as well as the ice surface velocity (Joughin et al., 2017) in a range of 54–64 m/a (velocity values lower than 54 m/a are transparent). Panel c shows the same velocity map together with the horizontal roughness η. Both roughness maps (b and c) show the hillshade of the bed elevation in the background. The red line on all three maps represents the location of the radar profile in Figure 4.

the basal topographic depression (R_{trough}) and is also characterized by lower vertical and horizontal roughness. Flowlines in Figure 5a show that ice surface flow in the eastern part of the region (yellow flow line in Figure 5a) deviates slightly toward south-east (orographic right) as it flows around the central ridge trough the topographic depression, whereas a flowline located north-west to the ridge bend less toward the trough (green flow line in Figure 5a).

3.3. Basal Return Power and Waveform Abruptness

In Figure 6, we present the BRP of the basal reflection in (dB) for profiles aligned along-flow (a) and across-flow (b). The BRP, which is corrected for spherical spreading and englacial attenuation (constant value of 8 dB per km ice thickness), varies in a range of −25 to 25 dB. The BRP for the area around the EGRIP drill site agrees with the data of Christianson et al. (2014) and Holschuh et al. (2019). These two studies analyzed the BRP in the immediate surrounding of the EGRIP drill site, which they characterized as high return power in the center of the ice stream, low return power in the area of the shear margins and again higher return power outside of the shear margins. In general, the BRP on along- and across-flow profiles within the ice stream is higher than outside. Highest BRP values on across-flow profiles are concentrated within a ∼10 km corridor in the center of the ice stream, and decrease toward the shear margins. Along-flow profiles in the upstream part, which are located inside of the ice stream, show a stronger BRP than profiles located outside of the ice stream. Downstream of the EGRIP drill site, where the ice stream is widening, high return power values of across-flow profiles are not constrained to the center of the ice stream. Further downstream, BRP in across-flow profiles is highest in the region of the topographic depression (R_{trough}), is lower on the central ridge and decreases toward the margins. The strongest drop of BRP in profiles parallel to flow profiles coincides with the location of the central ridge (ridge indicated in Figure 5a). However, be-
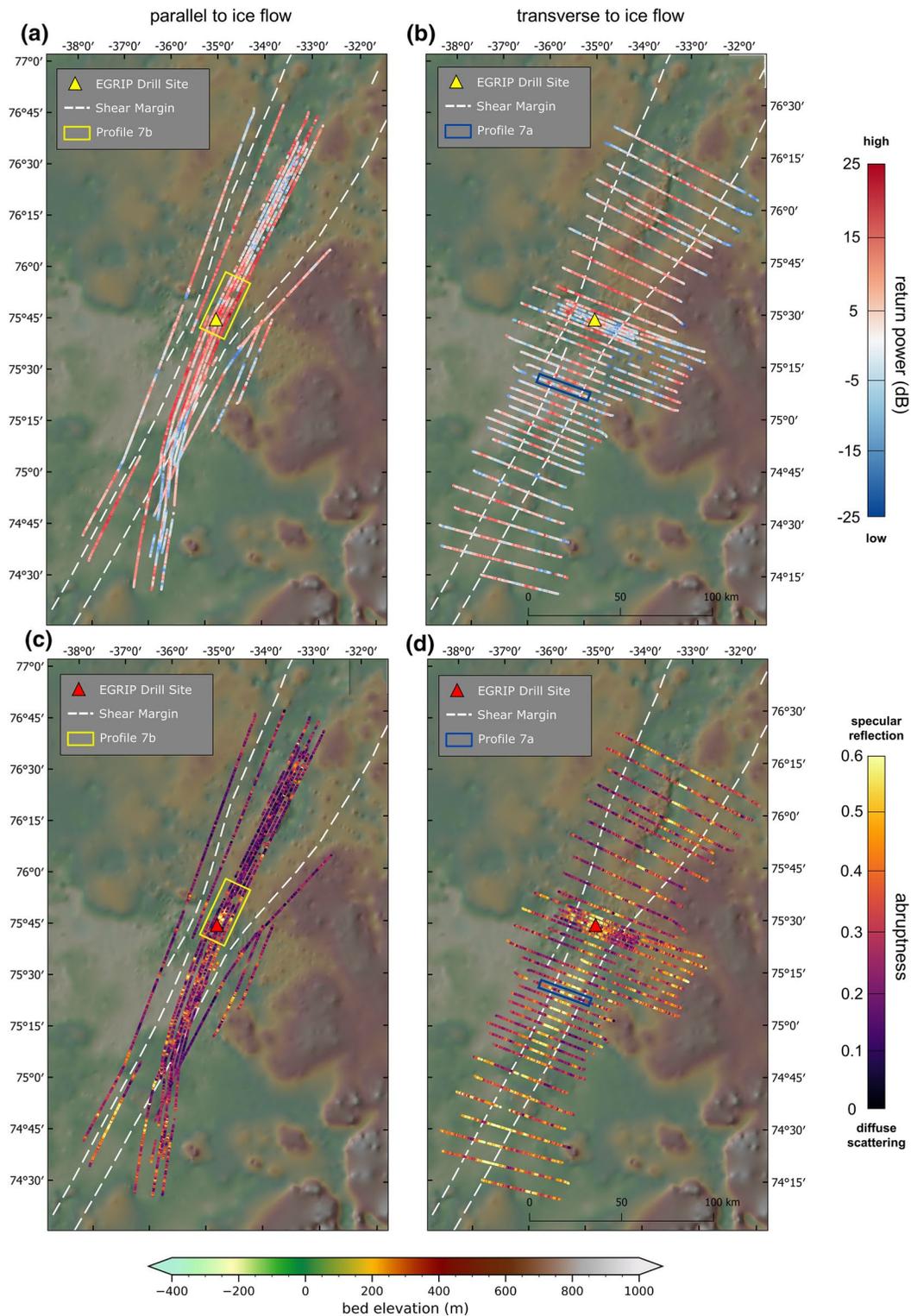
Figure 6. Bed echo characteristics for (a) and (b) basal return power and (c) and (d) waveform abruptness for profiles oriented along-flow (a) and (c) and across-flow (b) and (d), respectively. Basal return power is corrected for spherical spreading as well as englacial attenuation losses (8 dB/km ice thickness) and displayed in decibel (dB with respect to unity). Waveform abruptness is expressed as the ratio between the maximum BRP and the integrated bed return power and is thus unitless. High values (yellow) represent the dominance of specular reflection and low values (dark purple) the dominance of diffuse scattering of the base. The yellow and blue rectangular outlines indicate the position of the radargrams in Figure 7. The interpretation of bed permittivity from the BRP data presented here is limited due to the simple correction scheme for englacial attenuation applied here. A large part of the spatial heterogeneity in BRP probably results due to an inaccurate englacial attenuation correction, which cannot be overcome due to an uncertainty in englacial temperature distribution.

cause we use a constant correction factor for englacial attenuation, some of the variations in BRP might be introduced by this correction. It is very likely that the large heterogeneity in BRP is a result from this simple correction scheme.

Figures 6c and 6d show the spatial distribution of the waveform abruptness for along- and across-flow profiles, respectively. Abruptness values range from 0.03 to 0.6, where smaller values are associated with a dominance of diffuse scattering (e.g., off-nadir reflections from cross-track) and higher values with more specular reflections. Along-flow profiles show significantly lower average abruptness values than profiles oriented perpendicular to ice flow in both, the upstream and downstream region. Furthermore, along-flow profiles in the upstream region show slightly higher abruptness values than the downstream region. Across-flow profiles in Figure 6d show the highest values in the upstream survey area, which are concentrated in the center of the ice stream. This patch of high abruptness values has a similar extent as the patch of high basal return power in Figure 6b. Lower abruptness values in the upstream area are aligned in a zone extending 2–5 km from the shear margin to the ice stream center and outside of the shear margins. In the downstream area, high abruptness values are located in a zone of a localized topographic depression (R_{trough}) as well as in the immediate surrounding of the EGRIP drill site. Abruptness values in the downstream region, outside of these two areas are significantly lower. Values of BRP and waveform abruptness show a strong correlation in across-flow profiles but not as clear in along-flow profiles (high abruptness values with high BRP and low abruptness values with low BRP).

Two representative radargrams for the upstream and downstream region with their corresponding bed return power and abruptness are shown in Figure 7. Profile 7a shows high bed return power and high abruptness in the center of the ice stream (outlined with the black dashed line) and outside of the ice stream close to the shear margin (white and gray dashed line). The along-flow profile 7b in the center of the stream shows on average a constant high basal return power. Its waveform abruptness is on average higher between 0 and 12 km along-track and decreases thereafter. This change correlates with a step in the bed elevation, which marks a general change of the topographic regime.

3.4. Basal Water Routing

The subglacial water flux follows the gradient of the hydraulic potential. The direction of the water pathways is in general oriented toward the direction of ice flow and decreasing ice thickness (Figure 8). We compared subglacial water routing derived by the EGRIP-NOR-2018 bed elevation model and the BMv3 bed elevation model (blue and red lines in Figure 8, respectively). The general pattern is the same: In the upstream region, pathways that drain the largest area lead into the ice stream and flow around bed obstacles. About 20 km upstream of the EGRIP drill site, the main water pathways lead through the shear margins into the ice stream toward the point of lowest bed elevation. The pathway with the highest number of upstream routing cells is entering the ice stream from the South-East. About 10 km upstream of the EGRIP drill site the routing inside of the ice stream follows the south-eastern shear margin and propagates downstream. Pathways entering the ice stream at the north-western shear margin propagate along the shear margin downstream. At the location of the drill site, the ice stream widens from ~25 to ~60 km at the downstream end of our survey area and two dominant pathways develop in the ice stream: One on the south-eastern side of the ice stream with a higher number of upstream cells, and a second on the western side of the NEGIS. About 40 km downstream of EGRIP, the south-eastern path changes its location from the eastern shear margin to the local trough (our subregion R_{trough}), continuing in ice-flow direction and then switching its location back to the shear margin after another 40 km. The north-western pathway stays more or less in the area of the shear margin. Summarizing, the water routing in the downstream area seems to predominantly follow the location of the shear margins and local troughs in the bed topography in the ice stream.

We identify three locations where the routing pathways deviate significantly for the two topographies (features 1–3 in Figure 8). At all three features, the blue EGRIP-NOR-2018 water routing follows preferably the location of the shear margin outline, whereas the BMv3 routing deviates and flows toward the center of the ice stream.
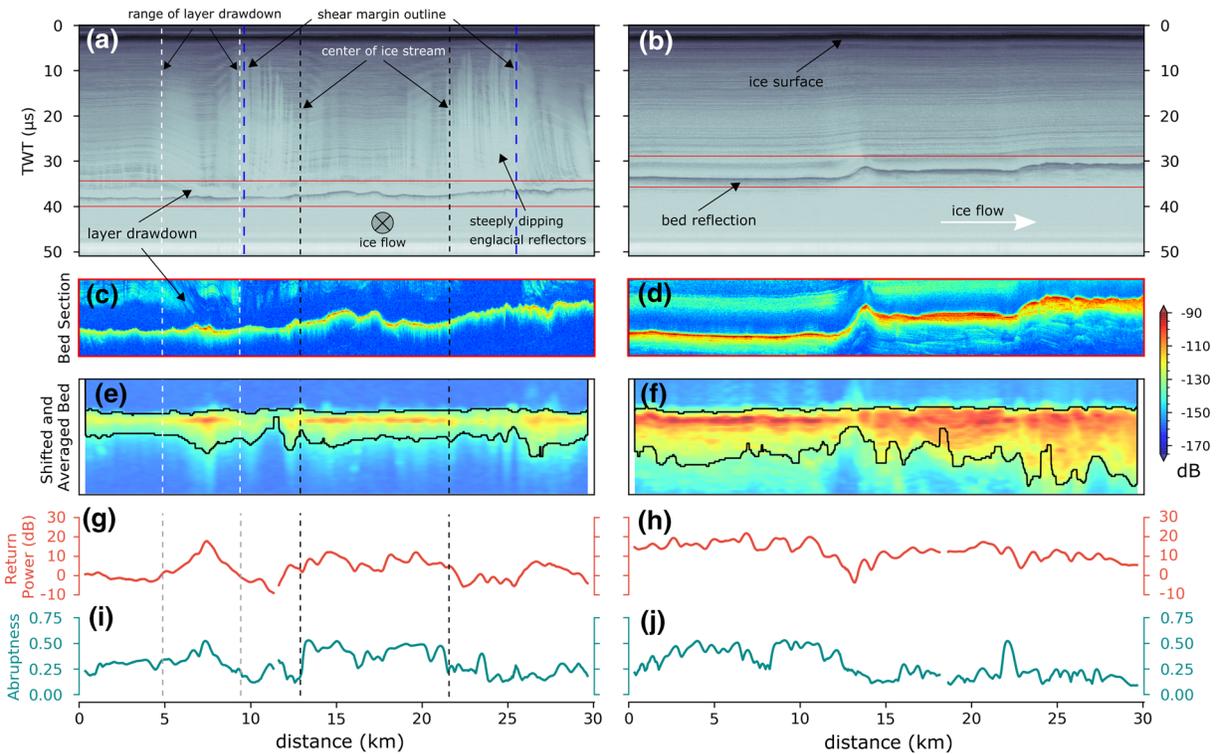
Figure 7. Two radar sections (two-way travel time (TWT) on the *y*-axis) and basal return echo properties from (a) an across-flow profile (location is indicated in Figures 6b and 6d with the blue outline) and (b) an along-flow profile (location is indicated in Figures 6a and 6c with the yellow outline). Panels c and d represent the analysis window of the ice-bed interface of the corresponding radargrams (indicated with the red lines in the radargrams) and their amplitude in dB. Panels e and f show the elevation-leveled basal reflectors and the corresponding BRP after along-track averaging. The black outline represents the window of integration for basal return power. The radargrams in panels a-f are neither corrected for spherical spreading nor englacial attenuation. Panels g and h show BRP corrected for spherical spreading as well as englacial attenuation (8 dB per km ice thickness) and (i) and (j) the waveform abruptness. The blue dashed lines in (a) show the position of the shear margins, the white dashed lines the region of layer drawdown outside of the shear margins and the black dashed lines the central part of the ice stream.

4. Discussion

The analysis and interpretation of the conditions of the ice base inferred by airborne radar sounding data are subject to several uncertainties resulting from radar data processing, the energy loss in the ice column as well as the interpretation of basal roughness parameters. We address these uncertainties in detail in the appendix. The uncertainties from each method affects the robustness of our interpretations with different significance. For example, the potential uncertainty of BRP due to the unknown variations in englacial temperature in our survey region has a much larger effect on the interpretation than the uncertainty of BRP caused by the roughness of the bed.

4.1. Interpretation of Large-Scale Basal Conditions

The observation of higher *large-scale* vertical roughness values in the faster-flowing area of our study region does not conform with the results of other subglacial roughness studies in West Antarctica (Bingham & Siegert, 2009; Diez et al., 2018; Rippin et al., 2014; Siegert et al., 2005, 2016). These studies conclude that fast ice flow is mostly topographically controlled and associated with a smooth bed, while slow-flowing areas are characterized by a rougher bed and the absence of a trough. Rippin et al. (2011) suggest that a smooth bed hints to a decrease of basal drag, favoring high ice-flow velocities. In contrast to our study, those study areas were concentrated mostly on the terminating part of glaciers. Therefore, we cannot directly relate to the interpretations from studies investigating outlet glaciers and ice streams. However, Holschuh et al. (2020) investigated Thwaites glacier several 100 km of the grounding line and find the area of lowest basal drag in the region of extremely rough bed topography.
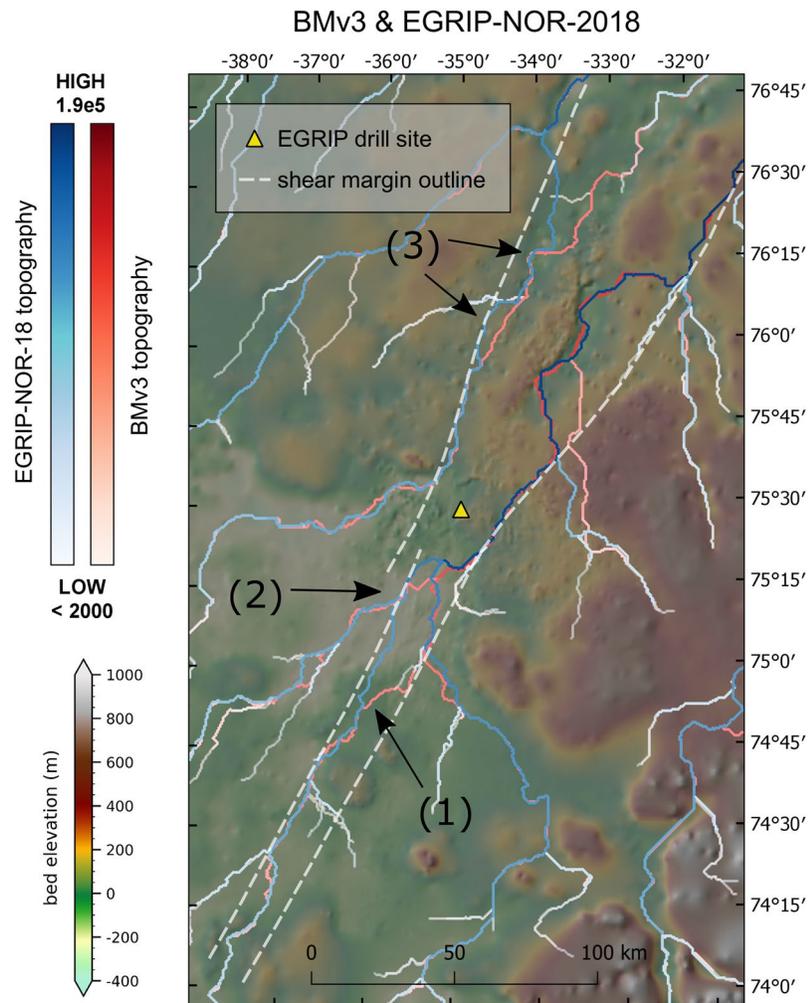
Figure 8. Basal water routing pathways calculated based on EGRIP-NOR-2018 bed elevation (Franke et al., 2020b; in blue) as well as pathways calculated with the bed elevation model BMv3 (Morlighem et al., 2017; in red). The basal water routing color saturation represents the number of accumulated upstream cells. Pixels containing less than 2,000 upstream cells are transparent. High values and dark colors represent pathways that transport larger amounts of upstream cells. Features (1)–(3) present locations where the routing pathways from the two bed elevation models show the largest deviations. The background map represents the bed elevation of the EGRIP-NOR-18 data.

The generally higher values of vertical roughness in across-flow profiles in comparison to along-flow profiles of ξ and η (Figures 9a and 9b) is an indication that the bed has been modified by ice flow. In the upstream region R_{up}, we find a trend toward higher vertical roughness in across-flow profiles inside and outside of the ice stream. A higher ξ in across-flow profiles could be an indication for streamlining of the bed in ice flow direction. The formation of elongated subglacial landforms with increasing ice flow velocities cannot be interpreted by our large-scale roughness values alone but is supported by the observations of Franke et al. (2020b), who interpret off-nadir side reflections as an indication for the presence of elongated subglacial landforms oriented parallel to ice flow.

Further downstream the ice stream slows down on its northern side due to a step in the bed topography and a general change of the terrain, which might be due to a change in bedrock type, and thus a higher mean vertical roughness, which is probably not related to ice flow. The analysis of flux gates shows that the additional incoming ice mass through the shear margins is evacuated by two different mechanisms. In the upstream regime we observe that flowlines converge (Figure 3), which is compensated by along-flow stretching due to ice stream acceleration. Downstream of flux gate 8, ice flow acceleration decreases, the ice
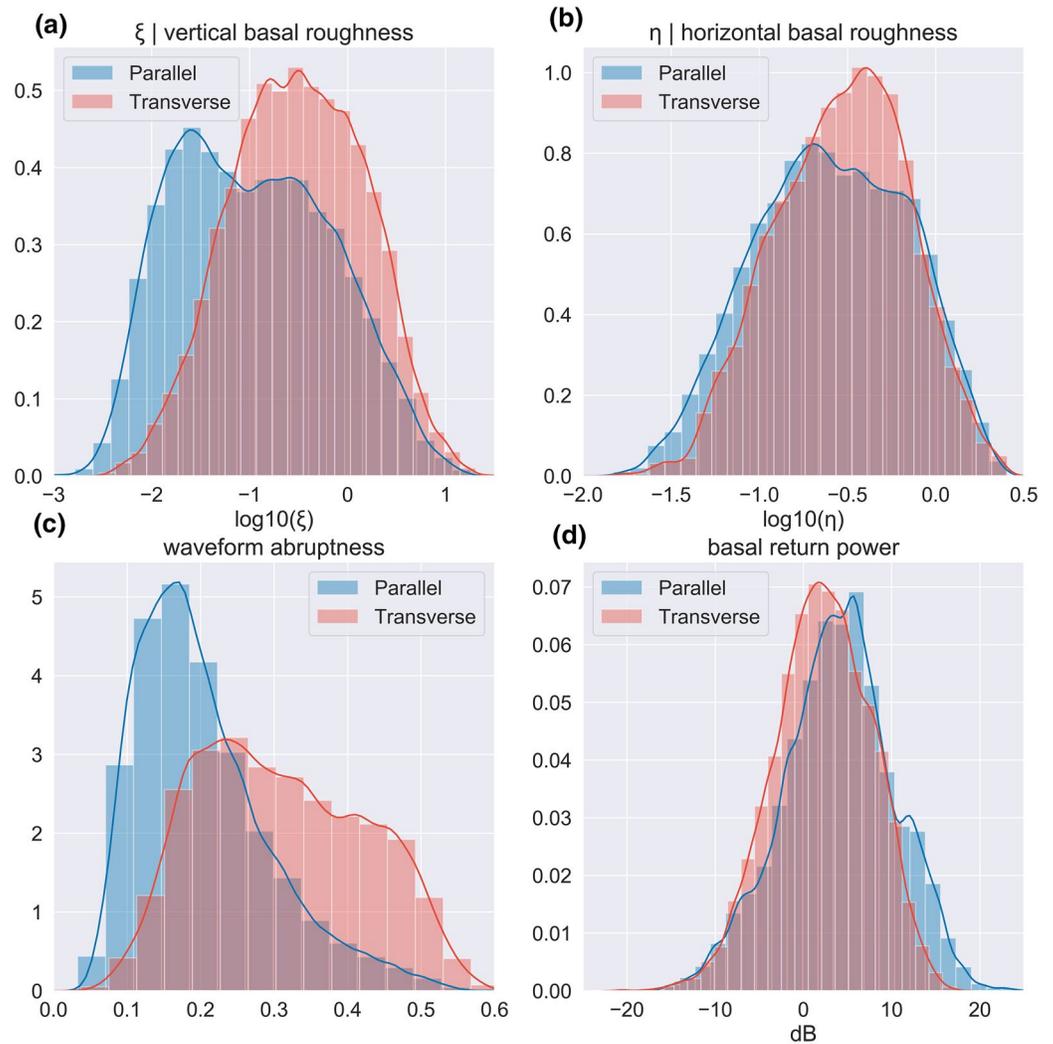
Figure 9. Histograms presenting the distribution of (a) vertical basal roughness, (b) horizontal basal roughness, (c) waveform abruptness, and (d) BRP for profiles oriented along- and across-flow for the location inside of the ice stream. The interpretation of anisotropy of BRP is limited due to the simple correction scheme for englacial attenuation. Blue bins represent along- and red bins across-flow profiles. The *y*-axis shows the kernel density estimation.

stream widens and flowlines do neither converge nor diverge. Hence, the widening of the ice stream has two interdependent effects: (i) excess ice mass can be evacuated without ice stream acceleration but also (ii) more ice is added to the system on a shorter distance due to the widening. Disregarding the initial cause for ice stream widening we observe a strong interdependence between the roughness of the bed, ice surface flow velocity and the geometry of the ice stream.

In contrast to the large-scale roughness, the small-scale roughness is defined by the reflection pattern and energy distribution of the bed echo. The resolution of a single point can range from ~ 60 m, which is the footprint of the Fresnel zone, to several 100s of meters if off-nadir side reflections interfere with the nadir return signal. For the analysis of the small-scale roughness, it is assumed that the energy reflected from a diffuse reflector in a large integration window should be proportional to the reflected energy of a specular target in a small window. The waveform abruptness is a measure for bed roughness in the across-track dimension of a radar profile. Low abruptness values indicate a rather diffuse reflection and high values a rather specular reflection transverse to the flight trajectory. If an intersection of two profiles shows a high value of *A* in an across-flow profile and a low *A* on an along-flow profile, we can infer a geomorphologic anisotropy, that

indicates streamlining in ice flow direction (Figure 9c). This anisotropy is significant in the center of the ice stream in the upstream region (Figures 6c and 6d) and supports the hypothesis of a streamlined bed.

Unlike the pattern in the waveform abruptness, we find no significant directional anisotropy in basal return power (Figure 9d). The basal return power can be influenced either by the scattering characteristics of the base, englacial energy loss due to folded internal layers or scattering, the thermal state of the ice as well as the availability and amount of liquid water at the base or a combination of these factors.

Englacial attenuation should be higher in the ice stream than in the surrounding ice (Matsuoka et al., 2012) and probably highest at the shear margin due to an increase in ice temperature by internal shear. It is likely that elevated temperatures in the margins do affect the BRP (see Holschuh et al., 2019). However, we have no evidence in our data to state if the increase in temperature is substantial to indicate temperate ice or the production of basal melt water. The existence of temperate ice in some regions would agree with a subglacial hydrology modeling study by Riverman et al. (2019). They suggested that subglacial bedforms in the shear margins are created by melt out of sediment within the ice column. The phenomenon described by Keisling et al. (2014) and Holschuh et al. (2014) of weak internal reflections at steeply dipping englacial reflectors in the shear margin area, as indicated in Figure 7a, does most likely have no effect on the BRP.

We find several indications that the BRP is influenced by the roughness of the bed. Within the ice stream area, we find higher BRP associated with high abruptness values in across-track profiles (see Figures 6b and 6d) as well as with low vertical roughness values (see Figure 2c). Low BRP on the central ridge in the downstream area is associated with low abruptness and high vertical roughness values in both along- and across-flow profiles. From this relationship we can interpret that the bed roughness can explain many of the changes in BRP inside of the ice stream. This interconnection was also observed by MacGregor et al. (2013) at the eastern shear margin at Thwaites Glacier.

The high BRP and low large- and small-scale roughness values in across-flow profiles in the center of region R_{up} could be interpreted as an indication for weak, porous, water saturated sediment, following similar interpretations of Rippin et al. (2011). As the modeled subglacial water routes suggest, it is possible that water is continuously channeled toward the ice stream and weakens the subglacial sediments, which could have a potential stabilizing effect on the ice flow (Bougamont et al., 2014). Our routing paths indicate that basal water does not leave the ice stream. Consequently, the base could become increasingly lubricated, reducing basal shear stress and facilitating basal slip.

The analysis of basal water routing shows that in the downstream region the water is distributed toward the shear margins. This pattern is much more consistent in the routing scheme calculated with the new high-resolution EGRIP-NOR-2018 bed topography than with BMv3. The additional radar data and the design of the EGRIP-NOR-2018 survey provide more details in the bed topography at the shear margins and inside of the ice stream than in previous models (Franke et al., 2020b). This highlights the importance of high-resolution bed elevation models to determine the subglacial water routing accurately and supports the hypothesis that the geometry of the NEGIS is strongly connected to the subglacial hydrology system (Perol et al., 2015).

Only a few regions in our survey area would be candidates for a topographically controlled positioning of the shear margins. Routing pathways indicate that basal water is distributed to both shear margins and propagates downstream directly along or in the vicinity of the position of the shear margins. If the position of the shear margins is particularly sensitive to the subglacial water pathways, it could facilitate the change of the location and the geometry of the NEGIS.

As the shear margins in the upstream regions of NEGIS appear not to be constrained by the bed topography or the basal substrate, their location might be fluctuating over time, allowing a more sensitive reaction to large-scale changes in the entire catchment area. Temporal variations in the surface slope of the ice sheet in Northeast Greenland, caused by changes in accumulation, distribution of surface melt or ocean forcing, can influence the subglacial water pathways (Karlsson & Dahl-Jensen, 2015). Hence, a warming climate with changes in the surface mass balance and characteristics in central Northeast Greenland may also influence the positioning of the shear margins of the NEGIS, or ice streaming in general.

4.2. Localized Geomorphological and Geological Features

The abrupt increase of ξ and η in region R_{down} is probably associated with a change in lithology because the roughness change coincides with a general change of topographic terrain properties. Downstream of the EGRIP drill site, the bed elevation is higher and the topography much more variable than upstream. A difference in horizontal roughness of the eastern (R_{east}) and the western region (R_{west}) of the downstream area (Figure 2d) as well as the local variations of vertical roughness in region R_{trough} (Figure 2c), could be explained by a different geomorphological setting. In this area, the interpretation scheme of Li et al. (2010) would explain the roughness distribution well. R_{east} shows a topographic depression and faster ice flow, low η and ξ could indicate material which is easier to erode. The geomorphic interpretation for the western region R_{west}, showing higher η and ξ, could be a mountainous setting with minor erosion and deposition of sediments and slower ice flow (Li et al., 2010). A setting similar to the downstream area of our survey region can be found in Antarctic ice streams: a central ridge oriented along-flow (Figure 5a), showing evidence for elongated subglacial landforms and indicating long term ice flow, and a several meters thick sediment. This has been reported for the Rutford ice stream (King et al., 2009) as well as Pine Island Glacier (Bingham et al., 2017; Brisbourne et al., 2017).

The increase of ξ along ice flow, the anisotropy of basal roughness, as well as the high waveform abruptness values in across-flow profiles within the ice stream in the upstream region R_{up}, indicate the development of elongated subglacial landforms inside of the ice stream. This is consistent with other observations (Christianson et al., 2014; Franke et al., 2020b). In several along-flow profiles on the central ridge in the downstream region R_{down}, we observe a side reflection pattern beneath the bed reflection, indicating side reflections of along-flow oriented structures (for details see Franke et al. (2020b)). Streamlined elongated bedforms in most cases consist of unconsolidated glacial sediments, were formed by fast streaming flow and are, thus, a record of former ice flow (Stokes & Clark, 2002). The pattern is similar to the bed striations found by Arnold et al. (2019), which are probably caused by glacier flow and suggest that elongated subglacial landforms are also present in this part of the survey area.

The appearance of elongated subglacial landforms can also occur at the shear margins of NEGIS. By analyzing seismic and radar data and modeling subglacial water flow, Riverman et al. (2019) find flow parallel features composed of saturated, soft, high-porosity till. Elongated subglacial landforms like mega-scale glacial lineation can form on soft beds, but also on hard-beds, although the generation of hard bed streamlining probably takes more time and/or higher ice flow velocities (Krabbendam et al., 2016). Because the ice surface velocities at the location where we interpret elongated subglacial landforms are comparably low, we argue that these landforms were probably generated on a soft and deformable bed. This interpretation is also in agreement with the findings of unconsolidated sediments of Christianson et al. (2014) inside and outside of the ice stream at the position where the ice stream widens. In the upstream region basal roughness patterns in along-flow profiles outside and inside the ice stream (Figures 2a and 2b) are similar, which indicates that the basal properties, and thus potentially basal substrate do not vary across the shear margins. Vallelonga et al. (2014) showed that sediments around the EGRIP drill site are present outside of the shear margin and suggested based on these findings, that the location of the shear margin could shift its location and maybe respond to a re-routing of basal water.

In the downstream region, we observe a decrease in velocity of the ice stream. Higher average vertical roughness contributes to an increase basal resistance and a slope in the bed topography decreases the local driving stress in this region. Around the location of the EGRIP Camp, the ice stream is widening and the ice thickness is reducing by ∼700 m. The thinning appears not to be uniform over the entire ice column, as the lowermost ice layer, until 200 m above bedrock, does not change its thickness (Figures 4a and 4e). Our flux analysis shows that the flux in the NEGIS ice stream is balanced by inflow through the shear margins. A vertically different response in flux indicates a change in the vertical velocity distribution. This could be interpreted as a transition in the stress regime from pure to simple shear at the base of the ice and thus less basal sliding. Indeed, a decrease in ice flow velocity can be observed at this location, which could be caused by a decrease in basal sliding. The basal unit retains its thickness for more than 100 km further along flow, which could be explained by decreased longitudinal stretching. This process would indicate an increased rate of internal deformation (Bons et al., 2018). An increase of internal shear and deformation within the ice column redistributes the shear strain from the ice-bed interface to within the ice column. Depending on

the localized basal shear stress and the basal flow velocity, which we are not able to quantify in this study, the basal ice temperature could be increased and eventually produce basal melt water.

The increase in BRP at locations where we also observe a drawdown of internal layers at the outer edges of the shear margins (e.g., Figures 7a and 7c) could be explained by two different mechanisms. Either, basal melting, and thus a wet base, which produces the drawdown of layers in the first place, increases BRP. However, we observe that deep layers outside of the ice stream appear at a higher elevation after they passed through the shear margin, which would contradict the mechanism of basal melting. It is also possible that the drawdown of internal layers moves colder ice masses downwards, which reduces the temperature of the ice close to the base and decreases englacial attenuation, potentially masking true changes in the BRP (Holschuh et al., 2019). High-resolution ice flow models and better estimates or measurements of the GHF are necessary to obtain a more reliable estimate of temperature distribution in the ice to correctly determine attenuation.

4.3. Synopsis of NEGIS Characteristics

A summary of the key findings and interpretations for the basal conditions of the NEGIS in the onset region are presented in Figure 10. Our results support the hypothesis and mechanisms proposed by Christianson et al. (2014). The predominant amount of ice mass flows into the ice stream through the shear margins. In the onset region of NEGIS, available meltwater and the presence of a soft, deformable bed provide lower resistance for sliding and facilitate accelerated ice flow. Given increasing velocities in the upstream region, the soft bed is most likely strongly deformable, leading to longitudinal geomorphological bedforms. In the upstream part, hydraulic pathways indicate that water is routed into the ice stream from neighboring areas. Further downstream, where the ice stream widens, basal water is pushed toward and beyond the shear margin, partly because of the local topography and lithological properties but also partly because of surface slopes of the ice surface. This leads to less resistant basal properties at the margins and enables a widening of the ice stream. Inside of the ice stream in the downstream area, high vertical roughness coincides with lower ice surface velocity and smooth areas with higher ice surface velocities. Both characteristics as well as the different thinning of internal layers are strong indications that basal shear stress is on average higher where the bed is rough. This could explain the non-uniform lateral ice surface velocities (feature three and four in the downstream region of Figure 10) and an increase in the rate of internal deformation of the basal ice unit (Figures 4a and 4e).

5. Conclusions

We characterized the basal properties of the onset region of NEGIS and discussed involved physical processes. The analysis of spectral basal roughness and basal return echoes shows a distinct change of basal conditions at the position where the ice stream widens. We conclude that a smooth, deformable, and lubricated base helps to initiate or at least favor ice flow acceleration at the onset of the NEGIS. The positioning of the shear margins and the pathways of subglacial water flow shows an immediate relationship between the ice stream extent and the subglacial hydrology system. Ice surface velocity, shear margin positioning and the pattern and intensity of the bed reflection are influenced by different scales of basal roughness. Regionally extending our interpretation, the involved processes could have a significant impact on the ice dynamics and ice stream catchments of Greenland in a warming climate. Changes in the surface mass balance in the upstream catchment, which is currently relatively small, could reorganize the location of the shear margins. It is possible that this could either initiate faster ice flow even further upstream, and/or take up a larger catchment area and, thus, increase the amount of ice discharge of the GrIS.

The drilling of the East Greenland Ice Core down to the bed will provide further insights into NEGIS' characteristics and dynamical processes, especially into fabric distribution, thermal structure, sediment properties and geothermal heat flux. As shown by our analyses, useful additional information to constrain the basal conditions can be provided by spatially extensive and closely spaced geophysical surveys. Considerable insights could be obtained by seismic soundings further upstream and downstream and borehole drillings to the base. However, these are time-consuming and expensive to acquire over a large area. To fully constrain the basal boundary conditions for ice flow models, a sufficient coverage of the middle and lower sections of NEGIS are needed.
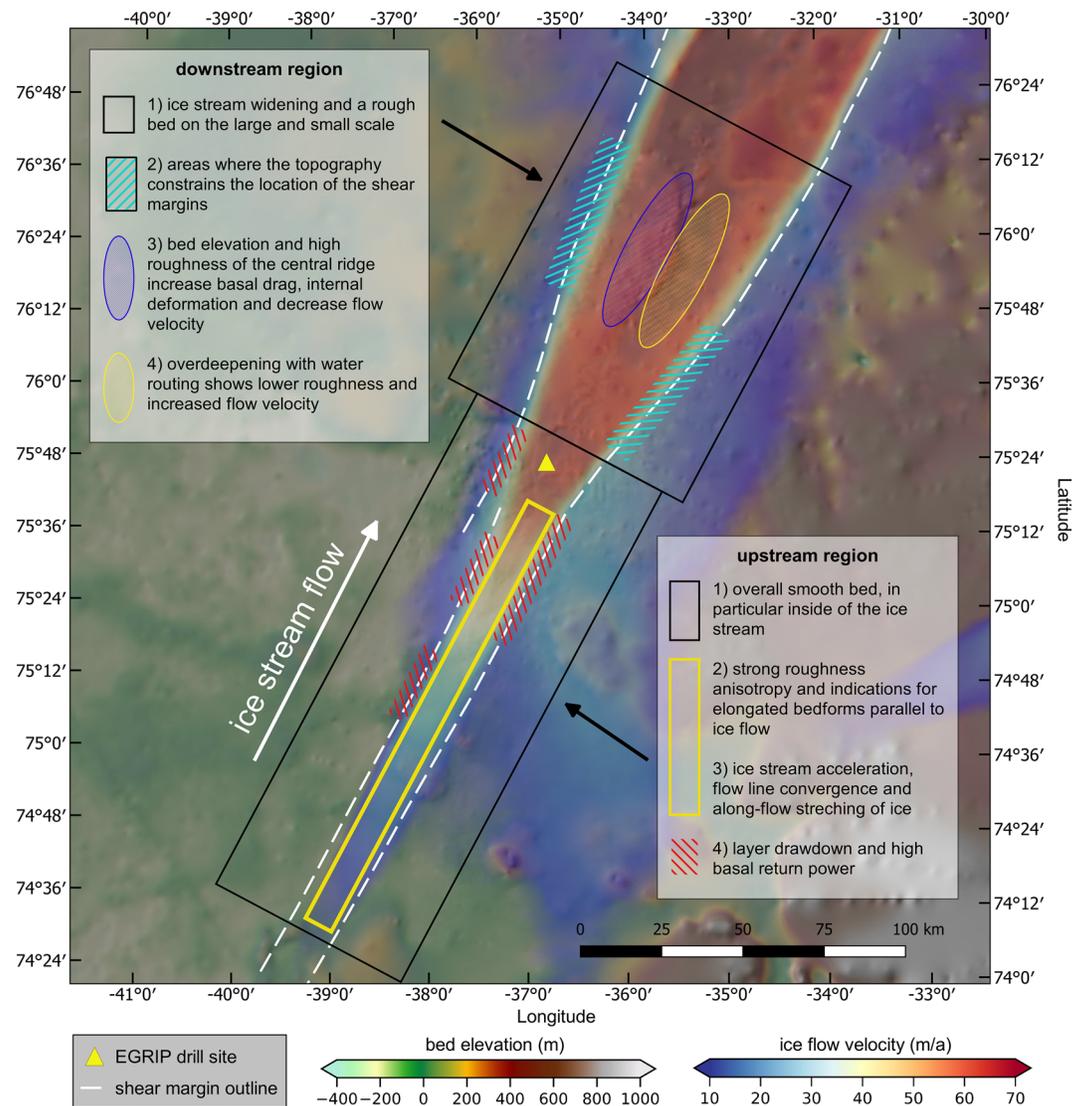
Figure 10. Summary of the basal properties of the upstream and the downstream survey region.

Appendix:

Uncertainties

Several uncertainties can influence the results and interpretation of the spectral bed roughness parameters. This accounts in particular for small values of ξ in conjunction with η. A major uncertainty arises from missing or ambiguous bed reflections and how continuous the tracking of the basal event is applied. In rough terrains, automatic trackers, for example, of reflection power, often create zigzag or step patterns whereas manual picking is often characterized by straight lines. A combination of both methods may represent the best possible way to pick the bed geometry efficiently. Still, it will have an impact on both vertical and horizontal roughness values, in particular when ξ is small. The uncertainty decreases if larger vertical amplitudes come into play. Li et al. (2010) introduced schematic interpretations for geomorphic settings based on the combination of ξ and η, which we will refer to as cases in the following. For example, low ξ and high η (case 1) can refer to a marine setting with intensive deposition of sediments. Low ξ and low η (case

2) could imply a continental setting after intensive erosion. For minimal values of ξ, this categorization is accompanied with a high uncertainty based on the radar data or bed topography product and the method of the ice-bed interface detection. For example, automatic or semiautomatic picking with a maximum power tracker might lead to a high-frequency zigzag pattern leading to case 2 (erosion). Manual picking at locations where a tracker is not useful can smooth the surface and would favor case 1 (deposition). Therefore, we argue that an interpretation of subglacial landscapes with low ξ are difficult to interpret in combination with η, even though the bed reflection is quality checked and picked very accurately. A robust interpretation of small ξ, regardless of high or low η, is that the base is smooth. Without additional data like radar wave scattering properties, seismic information about the basal substrate's lithology, or an indication for the presence of water at the base, further interpretations have low confidence. Another source of uncertainty are off-nadir/side reflections that are difficult to distinguish from nadir reflections. Only coherent and phase-sensitive radar depth sounders with multiple cross-track antenna elements and appropriate 3D processing algorithms can compute the direction angle of the reflected signal (Paden et al., 2010). A better estimate of the effect of cross-track roughness is the scattering-derived waveform abruptness (Cooper et al., 2019; Jordan et al., 2017; Oswald & Gogineni, 2008). However, this method does not consider side reflections from far off-nadir angles.

Several uncertainties in the BRP result from the mostly unobserved physical bulk properties of the ice column and their lateral variation, mainly across the ice stream. We anticipate an effect of ice crystal anisotropy on the basal return signal due to a different expected preferred orientation in the crystal fabric in the ice stream, outside of the ice stream, and in the area of the shear margins. However, overall we consider it as a negligible effect on the BRP (Matsuoka, 2011), given the magnitude of other uncertainties. The most significant uncertainty will arise from the unknown dielectric attenuation of the ice column from impurity loading and temperature, which is difficult to estimate for an ice stream. It is challenging to estimate the effect of englacial attenuation in our survey area because ice temperature has not been sufficiently constrained yet. For an ice stream, we have to consider three different lateral domains, with unknown dielectric attenuation: the fast-flowing central part of streaming ice, the slow-flowing part outside of the ice stream and the shear margins. Finally, in general, a layer of temperate ice of finite thickness might be present above the bed (Humbert et al., 2018). As we cannot constrain its presence further because of missing measurements, we do not consider it in our evaluation. An additional feature, influencing the bed return intensity can be internal layers of altered ice or containing entrainments of basal material which reduce the return energy of the bed. We find areas of large folds south-west of the EGRIP drill site outside of the ice stream. Therefore, we excluded this region because the strong internal deformation and bed entrainments appear to disturb the reflection power of the base significantly.

Further uncertainties are related to data acquisition and processing. Another source of uncertainty for the BRP can arise during SAR processing of the radar data. Focusing of scattered signals effectively shifts energy from multiple unfocused pixels into a single pixel. As a consequence, poor focusing due to position errors or directional scattering may cause the return power to deviate from the ideal case. Furthermore, the steeply dipping reflectors due to englacial layer folding in the vicinity of the shear margins will most likely reduce the reflected energy from the ice-basal interface underneath this zone. The energy loss probably occurs due to destructive interference in trace stacking, energy dispersion through SAR processing and off-nadir ray path losses (see Holschuh et al., 2014 for details).

Data Availability Statement

References

An, Lu, Rignot, E., Chauche, N., Holland, D. M., Holland, D., Jakobsson, M., et al. (2019). Bathymetry of Southeast Greenland from Oceans Melting Greenland (OMG) data. *Geophysical Research Letters*, *46*(20), 11197–11205. https://doi.org/10.1029/2019gl083953

Arndt, J. E., Larter, R. D., Hillenbrand, C.-D., Sørli, S. H., Forwick, M., Smith, J. A., et al. (2020). Past ice sheet–seabed interactions in the Northeastern Weddell sea embayment, Antarctica. *The Cryosphere*, *14*(6), 2115–2135. https://doi.org/10.5194/tc-14-2115-2020

Arnold, E., Leuschen, C., Rodriguez-Morales, F., Li, J., John, P., Hale, R., et al. (2019). CReSIS airborne radars and platforms for ice and snow sounding. *Annals of Glaciology*, 1–10. https://doi.org/10.1017/aog.2019.37

Aschwanden, A., Fahnestock, M. A., & Martin, T. (2016). Complex Greenland outlet glacier flow captured. *Nature Communications*, *7*(1). https://doi.org/10.1038/ncomms10524

Bingham, R. G., & Siegert, M. J. (2009). Quantifying subglacial bed roughness in Antarctica: Implications for ice-sheet dynamics and history. *Quaternary Science Reviews*, *28*(3–4), 223–236. https://doi.org/10.1016/j.quascirev.2008.10.014

Bingham, R. G., & Siegert, M. J. (2007). Radar-derived bed roughness characterization of Institute and M¨oller ice streams West Antarctica, and comparison with Siple Coast ice streams. *Geophysical Research Letters*, *34*(21). https://doi.org/10.1029/2007gl031483

Bingham, R. G., Vaughan, D. G., King, E. C., Davies, D., Cornford, S. L., Smith, A. M., et al. (2017). Diverse landscapes beneath Pine Island Glacier influence ice flow. *Nature Communications*, *8*(1). https://doi.org/10.1038/s41467-017-01597-y

Bons, P. D., Kleiner, T., Llorens, M.-G., Prior, D. J., Sachau, T., Weikusat, I., et al. (2018). Greenland Ice Sheet: Higher nonlinearity of ice flow significantly reduces estimated basal motion. *Geophysical Research Letters*, *45*(13), 6542–6548. https://doi.org/10.1029/2018gl078356

Bougamont, M., Christoffersen, P., L Hubbard, A., Fitzpatrick, A. A., Doyle, S. H., & Carter, S. P. (2014). Sensitive response of the Greenland Ice Sheet to surface melt drainage over a soft bed. *Nature Communications*, *5*(1). https://doi.org/10.1038/ncomms6052

Brisbourne, A. M., Smith, A. M., King, E. C., Nicholls, K. W., Holland, P. R., & Makinson, K. (2014). Seabed topography beneath Larsen C Ice Shelf from seismic soundings. *The Cryosphere*, *8*(1), 1–13. https://doi.org/10.5194/tc-8-1-2014

Brisbourne, A. M., Smith, A. M., Vaughan, D. G., King, E. C., Davies, D., Bingham, R. G., et al. (2017). Bed conditions of Pine Island Glacier West Antarctica. *Journal of Geophysical Research: Earth Surface*, *122*(1), 419–433. https://doi.org/10.1002/2016jf004033

Calov, R., Beyer, S., Greve, R., Beckmann, J., Willeit, M., Kleiner, T., et al. (2018). Simulation of the future sea level contribution of Greenland with a new glacial system model. *The Cryosphere*, *12*(10), 3097–3121. https://doi.org/10.5194/tc-12-3097-2018

Christianson, K., Peters, L. E., Alley, R. B., Sridhar, A., Jacobel, R. W., Riverman, K. L., et al. (2014). Dilatant till facilitates ice-stream flow in northeast Greenland. *Earth and Planetary Science Letters*, *401*, 57–69. https://doi.org/10.1016/j.epsl.2014.05.060

Clarke, G. K. C. (2005). Subglacial processes. *Annual Review of Earth and Planetary Sciences*, *33*(1), 247–276. https://doi.org/10.1146/annurev.earth.33.092203.122621

Clark, C. D., & Meehan, R. T. (2001). Subglacial bedform geomorphology of the Irish Ice Sheet reveals major configuration changes during growth and decay. *Journal of Quaternary Science*, *16*(5), 483–496. https://doi.org/10.1002/jqs.627

Cochran, J. R., & Bell, R. E. (2012). Inversion of IceBridge gravity data for continental shelf bathymetry beneath the Larsen Ice Shelf Antarctica. *Journal of Glaciology*, *58*(209), 540–552. https://doi.org/10.3189/2012jog11j033

Cooper, M. A., Jordan, T. M., Schroeder, D. M., Siegert, M. J., Williams, C. N., & Bamber, J. L. (2019). Subglacial roughness of the Greenland Ice Sheet: Relationship with contemporary ice velocity and geology. *The Cryosphere*, *13*(11), 3093–3115. https://doi.org/10.5194/tc-13-3093-2019

Corr, H., Moore, J. C., & Nicholls, K. W. (1993). Radar absorption due to impurities in Antarctic ice. *Geophysical Research Letters*, *20*(11), 1071–1074. https://doi.org/10.1029/93gl01395

Diez, A., Matsuoka, K., Ferraccioli, F., Jordan, T. A., Corr, H. F., Kohler, J., et al. (2018). Basal settings control fast ice flow in the recovery/slessor/bailey region East Antarctica. *Geophysical Research Letters*, *45*(6), 2706–2715. https://doi.org/10.1002/2017gl076601

Dowdeswell, J. A., Cofaigh, C. Ó, & Pudsey, C. J. (2004). Thickness and extent of the subglacial till layer beneath an Antarctic paleo–ice stream. *Geology*, *32*(1), 13. https://doi.org/10.1130/g19864.1

Dow, C. F., Hubbard, A., Booth, A. D., Doyle, S. H., Gusmeroli, A., & Kulessa, B. (2013). Seismic evidence of mechanically weak sediments underlying Russell Glacier West Greenland. *Annals of Glaciology*, *54*(64), 135–141. https://doi.org/10.3189/2013aog64a032

Dow, C. F., Karlsson, N. B., & Werder, M. A. (2018). Limited impact of subglacial supercooling freeze-on for Greenland ice sheet stratigraphy. *Geophysical Research Letters*, *45*(3), 1481–1489. https://doi.org/10.1002/2017GL076251

Durand, G., Gagliardini, O., Favier, L., Zwinger, T., & le Meur, E. (2011). Impact of bedrock description on modeling ice sheet dynamics. *Geophysical Research Letters*, *38*(20). https://doi.org/10.1029/2011gl048892

Eisen, O., Winter, A., Daniel, S., Kleiner, T., & Humbert, A. (2020). Basal roughness of the east antarctic ice sheet in relation to flow speed and basal thermal state. *Annals of Glaciology*, *61*(81), 162–175. https://doi.org/10.1017/aog.2020.47

Eisermann, H., Eagles, G., Ruppel, A., Smith, E. C., & Jokat, W. (2020). Bathymetry beneath ice shelves of western Dronning Maud land, east Antarctica, and implications on ice shelf stability. *Geophysical Research Letters*, *47*(12), e2019GL086724. https://doi.org/10.1029/2019GL086724

Fahnestock, M. (2001). High geothermal heat flow basal melt, and the origin of rapid ice flow in central Greenland. *Science*, *294*(5550), 2338–2342. https://doi.org/10.1126/science.1065370

Fahnestock, M., Bindschadler, R., Kwok, R., & Jezek, K. (1993). Greenland Ice Sheet surface properties and ice dynamics from ERS-1 SAR imagery. *Science*, *262*(5139), 1530–1534. https://doi.org/10.1126/science.262.5139.1530

Falcini, F. A. M., Rippin, D. M., Krabbendam, M., & Selby, K. A. (2018). Quantifying bed roughness beneath contemporary and palaeo-ice streams. *Journal of Glaciology*, *64*(247), 822–834. https://doi.org/10.1017/jog.2018.71

Franke, S., Jansen, D., Beyer, S., John, P., & Eisen, O. (2020a). *Basal conditions of the onset zone of the Northeast Greenland Ice Stream derived from airborne ultra-wideband radar data*. PANGAEA. https://doi.org/10.1594/PANGAEA.915136

Franke, S., Jansen, D., Binder, T., Dörr, N., John, P., et al. (2020b). Bed topography and subglacial landforms in the onset region of the Northeast Greenland Ice Stream. *Annals of Glaciology*, *61*(81), 143–153. https://doi.org/10.1017/aog.2020.12

Franke, S., Jansen, D., Binder, T., Dörr, N., John, P., Helm, V., et al. (2019). *Bedrock topography and ice thickness in the onset region of the Northeast Greenland Ice Stream recorded with the airborne AWI Ultra-Wideband radar (UWB) in 2018*. https://doi.pangaea.de/10.1594/PANGAEA.907918

Fretwell, P., Pritchard, H. D., Vaughan, D. G., Bamber, J. L., Barrand, N. E., Bell, R., et al. (2013). Bedmap2: improved ice bed surface and thickness datasets for Antarctica. *The Cryosphere*, *7*(1), 375–393. https://doi.org/10.5194/tc-7-375-2013

Förste, C., Schmidt, R., Stubenvoll, R., Flechtner, F., Meyer, U., Rolf, K. ¨onig, et al. (2007). The GeoForschungsZentrum Potsdam/Groupe de Recherche de Gèodésie Spatiale satellite-only and combined gravity field models: EIGEN-GL04S1 and EIGEN-GL04C. *Journal of Geodesy*, *82*(6), 331–346. https://doi.org/10.1007/s00190-007-0183-8

Gudlaugsson, E., Humbert, A., Winsborrow, M., & Andreassen, K. (2013). Subglacial roughness of the former Barents Sea ice sheet. *Journal of Geophysical Research: Earth Surface*, *118*(4), 2546–2556. https://doi.org/10.1002/2013jf002714

Hale, R., Miller, H., Gogineni, S., Yan, J. B., Rodriguez-Morales, F., Leuschen, C., et al. (2016). Multi-channel ultra-wideband radar sounder and imager. *2016 IEEE international geoscience and remote sensing symposium (IGARSS)*. IEEE. https://doi.org/10.1109/igarss.2016.7729545

Hofstede, C., Christoffersen, P., Hubbard, B., Doyle, S. H., Young, T. J., Diez, A., et al. (2018). Physical conditions of fast glacier flow: 2. Variable extent of Anisotropic Ice and soft basal sediment from seismic reflection data acquired on store glacier West Greenland. *Journal of Geophysical Research: Earth Surface*, *123*(2), 349–362. https://doi.org/10.1002/2017jf004297

Holschuh, N., Christianson, K., Paden, J., Alley, R. B., & Anandakrishnan, S. (2020). Linking postglacial landscapes to glacier dynamics using swath radar at Thwaites Glacier Antarctica. *Geology*. https://doi.org/10.1130/g46772.1

Holschuh, N., Christianson, K., & Sridhar, A. (2014). Power loss in dipping internal reflectors imaged using ice-penetrating radar. *Annals of Glaciology*, *55*(67), 49–56. https://doi.org/10.3189/2014aog67a005

Holschuh, N., Christianson, K., Sridhar, A., Alley, R. B., & Jacobel, R. W. (2016). Constraining attenuation uncertainty in common midpoint radar surveys of ice sheets. *Journal of Geophysical Research: Earth Surface*, *121*(10), 1876–1890. https://doi.org/10.1002/2016JF003942

Holschuh, N., Lilien, D., & Christianson, K. (2019). Thermal weakening, convergent flow, and vertical heat transport in the northeast Greenland Ice Stream shear margins. *Geophysical Research Letters*, *46*, 8184–8193. https://doi.org/10.1029/2019GL083436

Hubbard, B., Siegert, M. J., & McCarroll, D. (2000). Spectral roughness of glaciated bedrock geomorphic surfaces: Implications for glacier sliding. *Journal of Geophysical Research*, *105*(B9), 21295–21303. https://doi.org/10.1029/2000jb900162

Hughes, T., Sargent, A., & Fastook, J. (2011). Ice-bed coupling beneath and beyond ice streams: Byrd Glacier Antarctica. *Journal of Geophysical Research*, *116*(F3). https://doi.org/10.1029/2010jf001896

Humbert, A., Daniel, S., Helm, V., Beyer, S., & Kleiner, T. (2018). Missing evidence of widespread subglacial lakes at recovery glacier Antarctica. *Journal of Geophysical Research: Earth Surface*, *123*(11), 2802–2826. https://doi.org/10.1029/2017jf004591

Jacobel, R. W., Lapo, K. E., Stamp, J. R., Youngblood, B. W., Welch, B. C., & Bamber, J. L. (2010). A comparison of basal reflectivity and ice velocity in East Antarctica. *The Cryosphere*, *4*(4), 447–452. https://doi.org/10.5194/tc-4-447-2010

Jordan, T. M., Bamber, J. L., Williams, C. N., Paden, J. D., Siegert, M. J., Huybrechts, P., et al. (2016). An ice-sheet-wide framework for englacial attenuation from ice-penetrating radar data. *The Cryosphere*, *10*(4), 1547–1570. https://doi.org/10.5194/tc-10-1547-2016

Jordan, T. M., Cooper, M. A., Schroeder, D. M., Williams, C. N., Paden, J. D., Siegert, M. J., et al. (2017). Self-affine subglacial roughness: Consequences for radar scattering and basal water discrimination in northern Greenland. *The Cryosphere*, *11*(3), 1247–1264. https://doi.org/10.5194/tc-11-1247-2017

Jordan, T. M., Williams, C. N., Schroeder, D. M., Martos, Y. M., Cooper, M. A., Siegert, M. J., et al. (2018). A constraint upon the basal water distribution and thermal state of the Greenland Ice Sheet from radar bed echoes. *The Cryosphere*, *12*(9), 2831–2854. https://doi.org/10.5194/tc-12-2831-2018

Joughin, I., Fahnestock, M., MacAyeal, D., Bamber, J. L., & Prasad, G. (2001). Observation and analysis of ice flow in the largest Greenland ice stream. *Journal of Geophysical Research: Atmospheres*, *106*(D24), 34021–34034. https://doi.org/10.1029/2001jd900087

Joughin, I., Smith, B. E., & Howat, I. M. (2017). A complete map of Greenland ice velocity derived from satellite data collected over 20 years. *Journal of Glaciology*, *64*(243), 1–11. https://doi.org/10.1017/jog.2017.73

Karlsson, N. B., & Dahl-Jensen, D. (2015). Response of the large-scale subglacial drainage system of Northeast Greenland to surface elevation changes. *The Cryosphere*, *9*(4), 1465–1479. https://doi.org/10.5194/tc-9-1465-2015

Keisling, B. A., Christianson, K., Alley, R. B., Peters, L. E., Christian, J. E. M., Sridhar, A., et al. (2014). Basal conditions and ice dynamics inferred from radar-derived internal stratigraphy of the northeast Greenland ice stream. *Annals of Glaciology*, *55*(67), 127–137. https://doi.org/10.3189/2014aog67a090

King, E. C., Hindmarsh, R. C. A., & Stokes, C. R. (2009). Formation of mega-scale glacial lineations observed beneath a West Antarctic ice stream. *Nature Geoscience*, *2*(8), 585–588. https://doi.org/10.1038/ngeo581

Krabbendam, M., Eyles, N., Putkinen, N., Bradwell, T., & Arbelaez-Moreno, L. (2016). Streamlined hard beds formed by palaeo-ice streams: A review. *Sedimentary Geology*, *338*, 24–50. https://doi.org/10.1016/j.sedgeo.2015.12.007

Kulessa, B., Hubbard, A. L., Booth, A. D., Bougamont, M., Dow, C. F., Doyle, S. H., et al. (2017). Seismic evidence for complex sedimentary control of Greenland Ice Sheet flow. *Science Advances*, *3*(8), e1603071. https://doi.org/10.1126/sciadv.1603071

Larour, E., Utke, J., Csatho, B., Schenk, A., Seroussi, H., Morlighem, M., et al. (2014). Inferred basal friction and surface mass balance of the Northeast Greenland Ice Stream using data assimilation of ICESat (Ice Cloud and land Elevation Satellite) surface altimetry and ISSM (Ice Sheet System Model). *The Cryosphere*, *8*(6), 2335–2351. https://doi.org/10.5194/tc-8-2335-2014

Layberry, R. L., & Bamber, J. L. (2001). A new ice thickness and bed data set for the Greenland ice sheet: 2. Relationship between dynamics and basal topography. *Journal of Geophysical Research: Atmospheres*, *106*(D24), 33781–33788. https://doi.org/10.1029/2001jd900053

Le Brocq, A. M., Payne, A. J., & Siegert, M. J. (2006). West Antarctic balance calculations: Impact of flux-routing algorithm smoothing algorithm and topography. *Computers & Geosciences*, *32*(10), 1780–1795. https://doi.org/10.1016/j.cageo.2006.05.003

Le Brocq, A. M., Payne, A. J., Siegert, M. J., & Alley, R. B. (2009). A subglacial water-flow model for West Antarctica. *Journal of Glaciology*, *55*(193), 879–888. https://doi.org/10.3189/002214309790152564

Li, X., Sun, Bo, Siegert, M. J., Bingham, R. G., Tang, X., Zhang, D., et al. (2010). Characterization of subglacial landscapes by a two-parameter roughness index. *Journal of Glaciology*, *56*(199), 831–836. https://doi.org/10.3189/002214310794457326

Livingstone, S. J., Clark, C. D., Woodward, J., & Kingslake, J. (2013). Potential subglacial lake locations and meltwater drainage pathways beneath the Antarctic and Greenland ice sheets. *The Cryosphere*, *7*(6), 1721–1740. https://doi.org/10.5194/tc-7-1721-2013

MacGregor, J. A., Catania, G. A., Conway, H., Schroeder, D. M., Joughin, I., Young, D. A., et al. (2013). Weak bed control of the eastern shear margin of Thwaites Glacier West Antarctica. *Journal of Glaciology*, *59*(217), 900–912. https://doi.org/10.3189/2013jog13j050

MacGregor, J. A., Fahnestock, M. A., Catania, G. A., Aschwanden, A., Clow, G. D., Colgan, W. T., et al. (2016). A synthesis of the basal thermal state of the Greenland Ice Sheet. *Journal of Geophysical Research: Earth Surface*, *121*(7), 1328–1350. https://doi.org/10.1002/2015jf003803

Macgregor, J. A., Li, J., Paden, J. D., Catania, G. A., Gary, D. C., Fahnestock, M. A., et al. (2015). Radar attenuation and temperature within the Greenland Ice Sheet. *Journal of Geophysical Research: Earth Surface*, 983–1008. https://doi.org/10.1002/2014JF003418

Matsuoka, K. (2011). Pitfalls in radar diagnosis of ice-sheet bed conditions: Lessons from englacial attenuation models. *Geophysical Research Letters*, *38*(5). https://doi.org/10.1029/2010gl046205

Matsuoka, K., Frank, P., Callens, D., & Conway, H. (2012). Radar characterization of the basal interface across the grounding zone of an ice-rise promontory in East Antarctica. *Annals of Glaciology*, *53*(60), 29–34. https://doi.org/10.3189/2012aog60a106

Meyer, C. R., Yehya, A., Minchew, B., & Rice, J. R. (2018). A model for the downstream evolution of temperate ice and subglacial hydrology along ice stream shear margins. *Journal of Geophysical Research: Earth Surface*, *123*(8), 1682–1698. https://doi.org/10.1029/2018jf004669

Minchew, B. M., Meyer, C. R., Pegler, S. S., Lipovsky, B. P., Rempel, A. W., Hilmar Gudmundsson, G., et al. (2019). Comment on "friction at the bed does not control fast glacier flow". *Science*, *363*(6427). https://doi.org/10.1126/science.aau6055

Morlighem, M., Rignot, E., Binder, T., Blankenship, D., Drews, R., Eagles, G., et al. (2019). Deep glacial troughs and stabilizing ridges unveiled beneath the margins of the Antarctic ice sheet. *Nature Geoscience*, *13*(2), 132–137. https://doi.org/10.1038/s41561-019-0510-8

Morlighem, M., Williams, C. N., Rignot, E., An, L., Arndt, J. E., Bamber, J. L., et al. (2017). BedMachine v3: Complete bed topography and ocean bathymetry mapping of Greenland from multibeam echo sounding combined with mass conservation. *Geophysical Research Letters*, *44*(21), 11051–11061. https://doi.org/10.1002/2017gl074954

Muto, A., Anandakrishnan, S., & Alley, R. B. (2013). Subglacial bathymetry and sediment layer distribution beneath the Pine Island Glacier ice shelf West Antarctica, modeled using aerogravity and autonomous underwater vehicle data. *Annals of Glaciology*, *54*(64), 27–32. https://doi.org/10.3189/2013aog64a110

Neckel, N., Drews, R., Rack, W., & Daniel, S. (2012). Basal melting at the Ekstr¨om Ice Shelf, Antarctica, estimated from mass flux divergence. *Annals of Glaciology*, *53*(60), 294–302. https://doi.org/10.3189/2012aog60a167

Oswald, G. K. A., & Gogineni, S. P. (2008). Recovery of subglacial water extent from Greenland radar survey data. *Journal of Glaciology*, *54*(184), 94–106. https://doi.org/10.3189/002214308784409107

Oswald, G. K. A., & Gogineni, S. P. (2012). Mapping basal melt under the northern Greenland ice sheet. *IEEE Transactions on Geoscience and Remote Sensing*, *50*(2), 585–592. https://doi.org/10.1109/tgrs.2011.2162072

Paden, J., Akins, T., Dunson, D., Allen, C., & Prasad, G. (2010). Ice-sheet bed 3-D tomography. *Journal of Glaciology*, *56*(195), 3–11. https://doi.org/10.3189/002214310791190811

Perol, T., Rice, J. R., Platt, J. D., & Jenny, S. (2015). Subglacial hydrology and ice stream margin locations. *Journal of Geophysical Research: Earth Surface*, *120*(7), 1352–1368. https://doi.org/10.1002/2015jf003542

Raney, R. K. (1998). The delay/Doppler radar altimeter. *IEEE Transactions on Geoscience and Remote Sensing*, *36*(5), 1578–1588. https://doi.org/10.1109/36.718861

Rippin, D. M. (2013). Bed roughness beneath the Greenland ice sheet. *Journal of Glaciology*, *59*(216), 724–732. https://doi.org/10.3189/2013jog12j212

Rippin, D. M., Bamber, J. L., Siegert, M. J., Vaughan, D. G., & Corr, H. F. J. (2006). Basal conditions beneath enhanced-flow tributaries of Slessor Glacier East Antarctica. *Journal of Glaciology*, *52*(179), 481–490. https://doi.org/10.3189/172756506781828467

Rippin, D. M., Bingham, R. G., Jordan, T. A., Wright, A. P., Ross, N., Corr, H. F. J., et al. (2014). Basal roughness of the Institute and M¨oller Ice Streams West Antarctica: Process determination and landscape interpretation. *Geomorphology*, *214*, 139–147. https://doi.org/10.1016/j.geomorph.2014.01.021

Rippin, D. M., Vaughan, D. G., & Corr, H. F. J. (2011). The basal roughness of Pine Island Glacier West Antarctica. *Journal of Glaciology*, *57*(201), 67–76. https://doi.org/10.3189/002214311795306574

Riverman, K. L., Sridhar, A., Alley, R. B., Holschuh, N., Dow, C. F., Muto, A., et al. (2019). Wet subglacial bedforms of the NE Greenland Ice Stream shear margins. *Annals of Glaciology*, *60*(80), 91–99. https://doi.org/10.1017/aog.2019.43

Rogozhina, I., Hagedoorn, J. M., Martinec, Z., Fleming, K., Soucek, O., Greve, R., et al. (2012). Effects of uncertainties in the geothermal heat flux distribution on the greenland ice sheet: An assessment of existing heat flow models. *Journal of Geophysical Research: Earth Surface*, *117*(F2). https://doi.org/10.1029/2011JF002098

Rosier, S. H. R., Hofstede, C., Brisbourne, A. M., Hattermann, T., Nicholls, K. W., Davis, P. E. D., et al. (2018). A new bathymetry for the Southeastern Filchner-Ronne ice shelf: Implications for modern oceanographic processes and glacial history. *Journal of Geophysical Research: Oceans*, *123*(7), 4610–4623. https://doi.org/10.1029/2018jc013982

Ryser, C., L¨uthi, M. P., Andrews, L. C., Catania, G. A., Funk, M., Hawley, R., et al. (2014). Caterpillar-like ice motion in the ablation zone of the Greenland ice sheet. *Journal of Geophysical Research: Earth Surface*, *119*(10), 2258–2271. https://doi.org/10.1002/2013jf003067

Schroeder, D. M., Bingham, R. G., Blankenship, D. D., Christianson, K., Eisen, O., Flowers, G. E., (2020). Five decades of radioglaciology. *Annals of Glaciology*, 1–13. https://doi.org/10.1017/aog.2020.11

Schroeder, D. M., Dowdeswell, J. A., Siegert, M. J., Bingham, R. G., Chu, W., MacKie, E. J., et al. (2019). Multidecadal observations of the Antarctic ice sheet from restored analog radar records. *Proceedings of the National Academy of Sciences*, *116*(38), 18867–18873. https://doi.org/10.1073/pnas.1821646116

Shepard, M. K., Campbell, B. A., Bulmer, M. H., Farr, T. G., Gaddis, L. R., & Plaut, J. J. (2001). The roughness of natural terrain: A planetary and remote sensing perspective. *Journal of Geophysical Research: Planets*, *106*(E12), 32777–32795. https://doi.org/10.1029/2000je001429

Shreve, R. L. (1972). Movement of water in glaciers. *Journal of Glaciology*, *11*(62), 205–214. https://doi.org/10.3189/s002214300002219x

Siegert, M. J., Ross, N., Li, J., Schroeder, D. M., Rippin, D., Ashmore, D., et al. (2016). Subglacial controls on the flow of Institute Ice Stream West Antarctica. *Annals of Glaciology*, *57*(73), 19–24. https://doi.org/10.1017/aog.2016.17

Siegert, M. J., Taylor, J., & Payne, A. J. (2005). Spectral roughness of subglacial topography and implications for former ice-sheet dynamics in East Antarctica. *Global and Planetary Change*, *45*(1–3), 249–263. https://doi.org/10.1016/j.gloplacha.2004.09.008

Smith-Johnsen, S., de Fleurian, B., Schlegel, N., & Nisanciolgu, K. (2019). Exceptionally high geothermal heat flux needed to sustain the northeast greenland ice stream. *The Cryosphere*. https://doi.org/10.5194/tc-2019-212

Smith-Johnsen, S., Schlegel, N.-J., Fleurian, B., & Nisancioglu, K. H. (2020). Sensitivity of the Northeast Greenland ice stream to geothermal heat. *Journal of Geophysical Research: Earth Surface*, *125*(1). https://doi.org/10.1029/2019jf005252

Smith, E. C., Hattermann, T., Kuhn, G., Gaedicke, C., Berger, S., Drews, R., et al. (2020). Detailed seismic bathymetry beneath ekstr¨om ice shelf, antarctica: Implications for glacial history and ice-ocean interaction. *Geophysical Research Letters*, *47*(10), e2019GL086187. https://doi.org/10.1029/2019GL086187

Smith, A. M., Jordan, T. A., Ferraccioli, F., & Bingham, R. G. (2013). Influence of subglacial conditions on ice stream dynamics: Seismic and potential field data from Pine Island Glacier West Antarctica. *Journal of Geophysical Research: Solid Earth*, *118*(4), 1471–1482. https://doi.org/10.1029/2012jb009582

Stearns, L. A., & van der Veen, C. (2019). Response to comment on "friction at the bed does not control fast glacier flow". *Science*, *363*(6427). https://doi.org/10.1126/science.aau8375

Stearns, L. A., & van der Veen, C. J. (2018). Friction at the bed does not control fast glacier flow. *Science*, *361*(6399), 273–277. https://doi.org/10.1126/science.aat2217

Stokes, C. R., & Clark, C. D. (2002). Are long subglacial bedforms indicative of fast ice flow?. *Boreas*, *31*(3), 239–249. https://doi.org/10.1111/j.1502-3885.2002.tb01070.x

Stokes, C. R., Spagnolo, M., Clark, C. D., Ó Cofaigh, C., Lian, O. B., & Dunstone, R. B. (2013). Formation of mega-scale glacial lineations on the Dubawnt Lake Ice Stream bed: 1. Size shape and spacing from a large remote sensing dataset. *Quaternary Science Reviews*, *77*, 190–209. https://doi.org/10.1016/j.quascirev.2013.06.003

Taylor, J., Siegert, M. J., Payne, A. J., & Hubbard, B. (2004). Regional-scale bed roughness beneath ice masses: Measurement and analysis. *Computers & Geosciences*, *30*(8), 899–908. https://doi.org/10.1016/j.cageo.2004.06.007

Vallelonga, P., Christianson, K., Alley, R. B., Anandakrishnan, S., Christian, J. E. M., Dahl-Jensen, D., et al. (2014). Initial results from geophysical surveys and shallow coring of the Northeast Greenland Ice Stream (NEGIS). *The Cryosphere*, *8*(4), 1275–1287. https://doi.org/10.5194/tc-8-1275-2014

Wilkens, N., Behrens, J., Kleiner, T., Rippin, D., Rückamp, M., & Humbert, A. (2015). Thermal structure and basal sliding parametrisation at Pine Island Glacier–a 3-D full-Stokes model study. *The Cryosphere*, *9*(2), 675–690. https://doi.org/10.5194/tc-9-675-2015

Winter, A., Daniel, S., Arnold, E. J., Blankenship, D. D., Cavitte, M. G. P., Corr, H. F. J., et al. (2017). Comparison of measurements from different radio-echo sounding systems and synchronization with the ice core at Dome C Antarctica. *The Cryosphere*, *11*(1), 653–668. https://doi.org/10.5194/tc-11-653-2017

Young, D. A., Schroeder, D. M., Blankenship, D. D., Kempf, S. D., & Quartini, E. (2016). The distribution of basal water between Antarctic subglacial lakes from radar sounding. *Philosophical Transactions of the Royal Society A: Mathematical, Physical & Engineering Sciences*, *374*(2059), 20140297. https://doi.org/10.1098/rsta.2014.0297